ATTENUATION IN IGNEOUS ROCKS

AT SEISMIC FREQUENCIES

by

HERMAN WILLIAM COOPER

B.Sc., Queen's University at Kingston
(1973)

M.Sc., Queen's University at Kingston
(1975)

SUBMITTED IN PARTIAL FULFILLMENT

OF THE REQUIREMENTS FOR THE

DEGREE OF

DOCTOR OF PHILOSOPHY

at the

 MASSACHUSETTS INSTITUTE OF TECHNOLOGY

August 1979

Signature of Author.....
Department of Earth and Planetary Sciences, August 28, 1979

Certified by.....
Thesis Supervisor

Accepted by.....
Chairman, Departmental Committee on Graduate Students

ATTENUATION IN IGNEOUS ROCKS

AT SEISMIC FREQUENCIES

by

Herman William Cooper

Submitted to the Department of Earth and Planetary Sciences August 28, 1979, in partial fulfillment of the requirements for the degree of Doctor of Philosophy.

ABSTRACT

Torsional attenuation measurements have been made on a set of igneous rocks at frequencies between 0.5 and 3.5 Hz under room dry and saturated conditions. Empirical relations between the specific dissipation factor Q^{-1} and crack porosity, η_c, of the rocks were found: $Q^{-1} = 0.17\sqrt{\eta_c}$ ±30% for the room dry rocks, and $Q^{-1} = 0.39\sqrt{\eta_c}$ ±40% for the saturated rocks. A model of attenuation due to friction on crack surfaces lubricated by thin films of adsorbed water is presented that can qualitatively account for the attenuation in nominally dry rocks and the effects of confining pressure, temperature, vacuum, and strain amplitude. A crack density and crack aspect ratio distribution for Westerly granite is used to show that a model of fluid flow between cracks, or squirt flow, can adequately account for the attenuation in saturated rocks at frequencies between 1 and 10^5 Hz. Attenuation mechanisms associated with cracks are important in the earth only in the upper 10 to 20 km. Inversions of surface wave attenuation data show that Q^{-1} of the crust under North America between 20 and 40 km is approximately 10^{-3}, consistent with laboratory measurements on essentially crack free rocks. Average crack porosities between 20 and 200×10^{-6} can explain the Q^{-1} of the upper 20 km of the crust.

Thesis Supervisor: Gene Simmons, Professor of Geophysics

ACKNOWLEDGEMENTS

I would like to express my gratitude to my advisor, Professor Gene Simmons, who proposed the topic of research amd made many helpful comments and suggestions during the preparation of this thesis.

During my first year at MIT I was supported by a Sloan Research Traineeship. This research was supported by the Division of Earth Sciences, National Science Foundation Grant 76-22130 EAR.

CONTENTS

TABLES

FIGURES

NOTATION

Symbols used only in Sec. 1.2 are not listed

a	half-length, or radius of a crack
a	sample radius
α	fraction of contact area S consisting of solid to solid contacts
A	oscillation amplitude
A	area of a crack
c	half-width of a crack
c_{44}, c_{55}, c_{66}	elastic moduli
E	Young's modulus of rock matrix
$\overline{E}$	effective Young's modulus of rock containing cracks
F	friction force
G	shear modulus
$\overline{G}$	effective shear modulus of rock containing cracks
J	moment of inertia
K	bulk modulus
K	torsional stiffness of cylinder
L	sample length
M	molecular weight
N	twisting couple
N_v	number of cracks per unit volume
p	vapour pressure
p_s	saturation vapour pressure

P	perimeter of a crack
P_c	crack closure pressure
P	yield stress
Q^{-1}	specific dissipation factor
Q_S^{-1}	Q^{-1} for shear waves
Q_P^{-1}	Q^{-1} for compressional waves
r_m	mean radius of curvature of a liquid surface
R	universal gas constant
s_{44}, s_{55}, s_{66}	elastic compliances
s_s	shear strength of solid junctions
s_ℓ	shear strength of boundary lubricant film
S	area of real contact between surfaces
S_i	strain components
T	temperature
T_i	stress components
u_1, u_2, u_3	displacements
v	volume of a crack
w	crack width
W	stored elastic energy
ΔW	energy loss per cycle
W	load
x_1, x_2, x_3	coordinates
z	thickness of adsorbed water layer
α	crack aspect ratio
β	compressibility
$\overline{\beta}$	effective compressibility of rock containing cracks
γ	surface tension

δ	angle
ε_{ij}	strain components
ϵ	crack density
ϵ'	density of cracks contributing to friction
ζ	linear strain attributable to the closure of cracks
ζ_v	volumetric strain attributable to crack closure
η	fluid viscosity
η_c	crack porosity
θ	angle of rotation
θ_c	contact angle between a liquid and a solid
μ	coefficient of friction
μ_s	coefficient of dry friction
μ_l	coefficient of friction when load is totally supported by lubricant film
ν	Poisson's ratio of rock matrix
$\bar{\nu}$	effective Poisson's ratio of rock containing cracks
ρ	fluid density
σ	normal stress acting on crack
τ	shear stress in the plane of a crack
τ_1	relaxation time for equalization of fluid pressure differences between cracks
τ_2	relaxation time for shear relaxation in pore fluid
ϕ	function describing the warping of the cross section of a cylinder in torsion
ψ	twist per unit length
ω	angular frequency

Chapter 1

INTRODUCTION

1.1 Objectives

The objectives of this work are:

1. To aid in understanding the mechanisms that cause seismic attenuation in rocks at temperatures and pressures corresponding to conditions in the upper crust of the earth. Much theoretical work has been done on the effects of cracks on attenuation, but few data have been available for rocks with well known crack characteristics.

2. To provide a set of data on cracked rocks to aid in the interpretation of seismic attenuation data. Detailed inversions of surface wave attenuation have shown that there are regional variations in Q^{-1} of the crust (Mitchell 1975, Canas and Mitchell 1978, Lee and Solomon 1979). The variations are probably due to regional differences in crack content or saturation.

1.2 Measures of attenuation

Several measures of attenuation are in general use. The one used here is Q^{-1}, sometimes called the specific dissipation factor. Its inverse, the seismic quality factor Q, used in earthquake seismology literature, is defined for a sinusoidal oscillation or travelling wave as

$$Q = \frac{2\pi W}{\Delta W} \tag{1.1}$$

where W is the maximum value of the elastic energy stored during a cycle and ΔW is the energy dissipated per cycle. From laboratory measurements, Q^{-1} can be defined either by the forced vibration method as

$$Q^{-1} = \frac{\Delta f}{f_n} \tag{1.2}$$

where Δf is the frequency width at half power of the resonance peak at frequency f_n; or from the decay of free vibrations, as in this work, as

$$Q^{-1} = \frac{1}{\pi f} \frac{d\ln A}{dt} \tag{1.3}$$

where f is the frequency and A is the amplitude of the vibration. Also used for free vibration measurements is the log decrement

$$\delta = \frac{\ln(A_1/A_2)}{(t_2-t_1)f} \tag{1.4}$$

where A_1 and A_2 are the amplitudes of the vibration at times t_1 and t_2. Comparing (1.3) with (1.4), we see that $Q^{-1} = \delta/\pi$. For small values of Q^{-1} ($<10^{-1}$), that is, $Q > 10$, the definitions (1.1), (1.2), and (1.3) are equivalent. The parameter used in wave propagation measurements is the attenuation coefficient α (γ is also used). For a plane wave,

$$\alpha = \frac{\ln(A_1/A_2)}{x_2 - x_1} \tag{1.5}$$

where A_1 and A_2 are the amplitudes of the wave at distances x_1 and x_2. The relation between Q^{-1} and α is

$$Q^{-1} = \frac{\alpha v}{\pi f} \qquad (1.6)$$

where v is the phase velocity of the wave. For a more detailed discussion of the various measures of attenuation, the experimental methods used to measure them, and their use in phenomological theories of anelastic behaviour, see Nowick and Berry (1972) and O'Connell and Budiansky (1978).

1.3 Previous experimental work

The following generalizations about attenuation in rocks can be made from the data reported in various studies, as has been pointed out by several authors (Knopoff 1964, Bradley and Fort 1966, Johnston et al 1979):

Frequency dependence. Q^{-1} has been found to be independent of frequency in dry rocks by many investigators:

1. between 10^{-3} and 6×10^{-2} Hz for a granite and a quartzite (Gordon and Davis 1968);
2. between 10^{-3} and 0.5 Hz for a granite and a diabase (Brennan and Stacey 1977);
3. between 40 and 120 Hz for six igneous and sedimentary rocks, with perhaps a 10% increase between 40 and 70 Hz (Bruckshaw and Mahanta 1954);
4. between 20 and 125 Hz for shear waves and between 50 and 450 Hz for compressional waves by field measurements in Pierre shale (McDonal et al 1958);
5. between 1 kHz and 10 kHz for shale and sandstone (Born 1941); and
6. between 50 kHz and 400 kHz in Westerly granite

(Knopoff and Porter 1963).

For fluid filled rocks fewer data are available. Born (1941) found that in Amherst sandstone containing 0.25% and 0.4% water by volume, Q^{-1} increased linearly with frequency between 600 and 1700 Hz. In contrast, Hamilton (1972) found a constant Q^{-1} between 3.5 kHz and 100 kHz from field measurements of compressional waves in marine sediments. A variation of Q^{-1} with frequency in saturated rocks is expected from fluid flow models of attenuation. A comparison of data at various single frequencies by several workers confirms this expectation. The ratios of Q^{-1} for saturated and dry rocks from Gardner et al (1964), Gordon and Davis (1968), Winkler and Nur (1979), and Toksoz et al (1979) are plotted in Fig. 1.1. If we assume that Q^{-1} for dry rocks is constant, then Q^{-1} for saturated rocks increases from the dry value at very low frequencies, reaches a peak between 10^3 and 10^5 Hz, then decreases again. The scatter may be due to differences in rock type, crack and pore porosity and geometry, amplitude of signals, and type of measurement. Gardner et al (1964) and Winkler and Nur (1979) found a larger ratio of Q^{-1} saturated to dry for extensional vibrations than for torsional vibrations in sandstones.

Effect of fluid. As shown in Fig. 1.1, the addition of fluid to a rock increases Q^{-1} except at very low frequencies. The amount of increase in Q^{-1} depends on the frequency and also on the degree of saturation. Gardner et al (1964) observed that most of the increase in Q^{-1} as fluid was added

Fig. 1.1. Variation of the ratio Q^{-1} saturated to Q^{-1} dry with frequency. Sources of the data: ●, O Gardner et al (1964); Δ Gordon and Davis (1968); ■, □ Winkler and Nur (1979); ◆, ◇ Toksoz et al (1979); ▼ this study. Filled symbols are measurements of shear oscillations or S waves; open symbols are measurements of extensional oscillations or P waves.

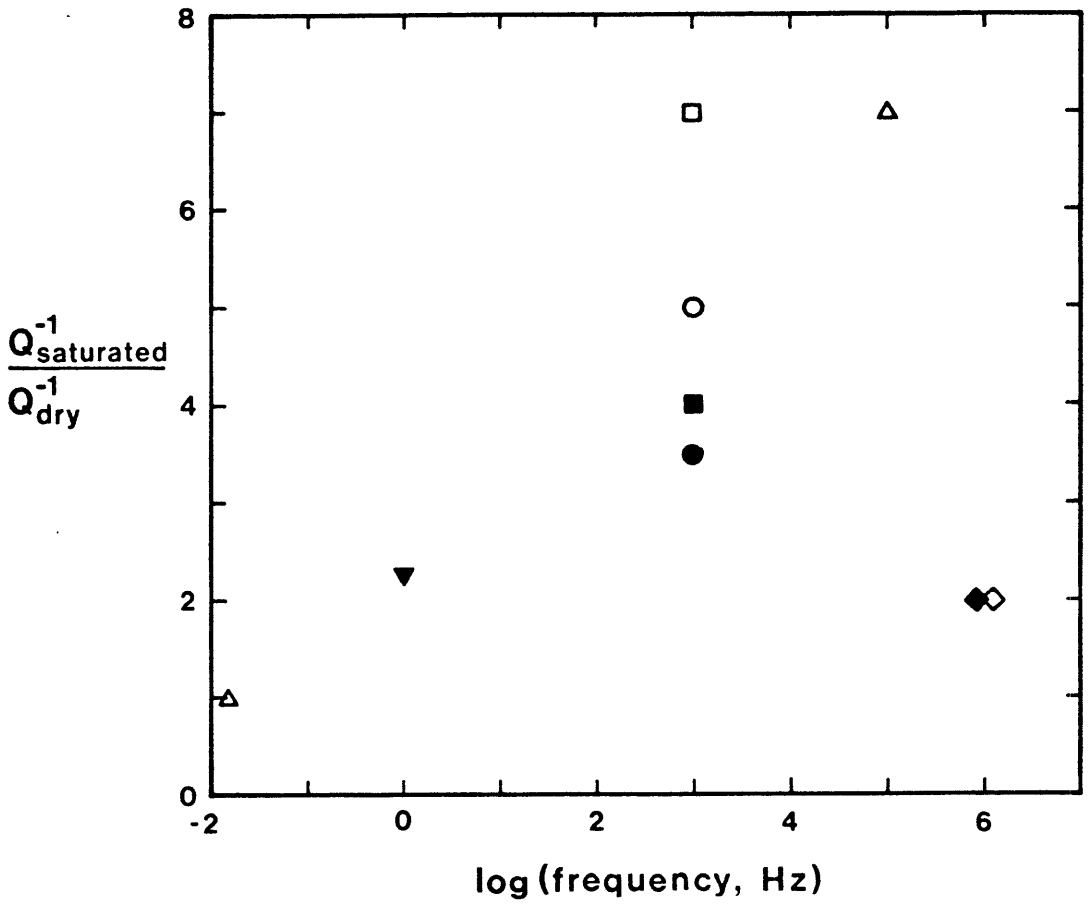
8
6
4
2
0
-2
0
2
4
6
$\frac{Q^{-1}_{saturated}}{Q^{-1}_{dry}}$
log (frequency, Hz)

to Berea sandstone occurred between saturations of 2% and 11% (see Fig. 1.2). Winkler and Nur (1979) observed that as saturation was changed from 95% to 100% in Massilon sandstone, Q^{-1} increased slightly for torsional vibrations but decreased slightly for extensional vibrations. Johnston (1978) found no significant difference in Q^{-1} between fully saturated and 37% saturated Berea sandstone for both shear and compressional waves, and in a gas release experiment found that Q^{-1} for compressional waves, Q_P^{-1}, increased slightly as a few percent gas bubbles were released into the pore fluid, but Q^{-1} for shear waves, Q_S^{-1}, remained constant. Frisillo and Stewart (1979) found that Q_P^{-1} in Berea sandstone was greatest at a fluid saturation of 65%.

The viscosity of the fluid also has an effect on attenuation. Gordon and Davis (1964) found no significant difference in Q^{-1} between dry and water saturated granite at 1.4×10^{-2} Hz, but granite saturated with glycerine had a higher, frequency dependent Q^{-1} between 10^{-3} and 1.4×10^{-2} Hz. By changing the temperature, Nur and Simmons (1969) varied the viscosity of glycerol saturating Barre granite. At 500 kHz they found a peak in Q_S^{-1} at a viscosity of approximately 0.2 poise, but no significant variation in Q_P^{-1}. Gordon (1974) reported a similar experiment using longitudinal oscillations at 50 kHz in which a peak in Q^{-1} occurred at a viscosity of 40 poise. In all theoretical models of fluid flow attenuation, viscosity enters as the product of viscosity and frequency. Therefore, variation of viscosity can also be

Fig. 1.2. Variation of extensional decrements of a Berea sandstone with overburden pressure at fixed water saturations. From Gardner et al (1964).

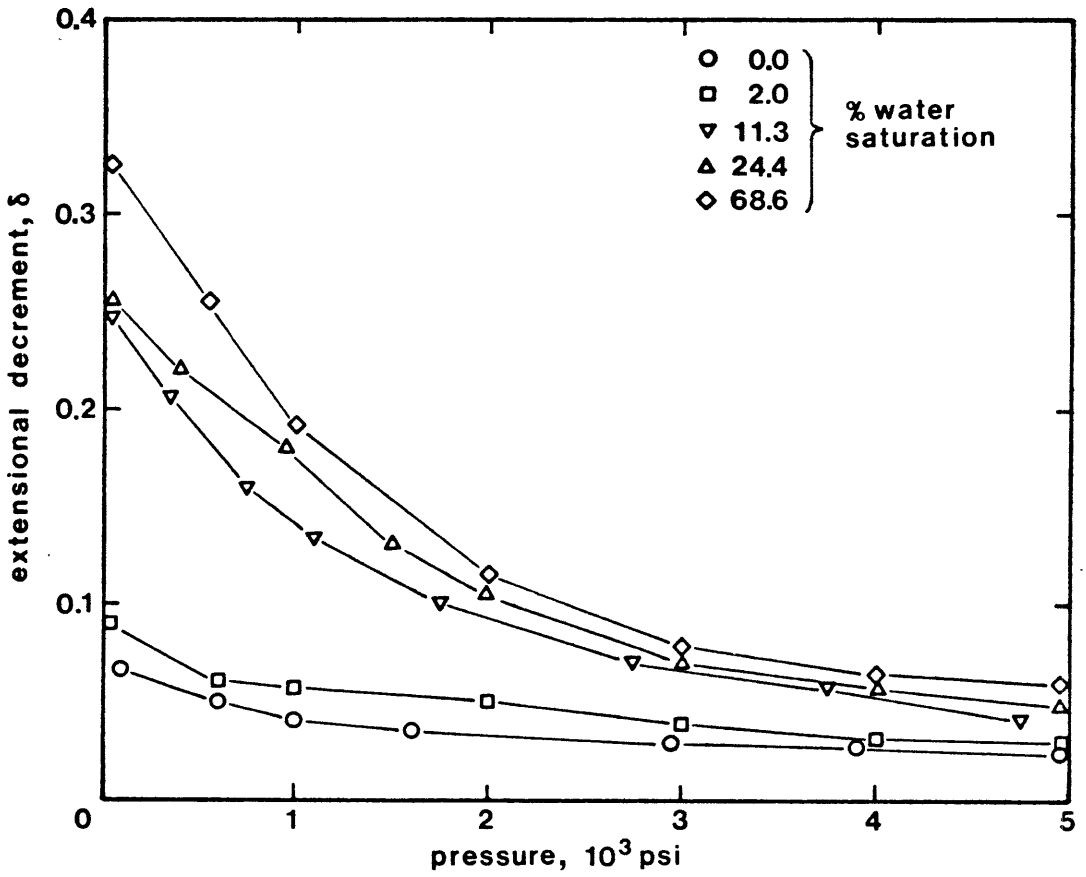
0.4
0.3
0.2
0.1
0
1
2
3
4
5
extensional decrement, δ
pressure, 10³ psi
0.0
2.0
11.3
24.4
68.6
% water saturation

considered as variation of the frequency for a given fluid viscosity. The effect of using a high viscosity fluid such as glycerine is to shift the fluid flow attenuation shown in Fig. 1.1 to lower frequencies.

At the other extreme of water content, Tittman et al (1975) reduced the Q^{-1} of a lunar basalt from 10^{-2} in lab atmosphere to 3×10^{-4} in a vacuum of 10^{-10} torr, with similar results for a terrestrial basalt (Tittman et al 1974). Recovery of the initial high value of Q^{-1} by re-exposure to lab atmosphere or water vapour shows that the attenuation in rocks normally called dry is caused somehow by adsorbed water vapour.

Effect of pressure. Several investigators have shown that Q^{-1} decreases for both rocks and unconsolidated sand as pressure is increased to between 300 bars to 1 kbar, after which Q^{-1} remains relatively constant as pressure is increased further (Gardner et al 1964, Gordon and Davis 1968, Winkler and Nur 1979, Toksoz et al 1979). The decrease in Q^{-1} is less pronounced for dry rocks than for saturated rocks. Figure 1.2 from Gardner et al (1964) shows typical results.

Effect of non-hydrostatic stress. Lockner et al (1977) applied an axial stress to a cylinder of Westerly granite and measured the changes in attenuation of P and S waves propagating normal to the stress axis. The attenuation of the S wave polarized parallel to the stress axis decreased as axial stress was increased until near failure, while the

attenuation of the P wave and the S wave polarized perpendicular to the stress axis remained relatively constant up to approximately half the failure strength and then increased at larger stress. Others have reported similar results. Gowd (1970) found that for propagation perpendicular to the stress axis, Q_p^{-1} decreased with stress up to half the failure strength and then increased with stress. Merkulova et al (1972) measured Q^{-1} of longitudinal oscillations in samples of gabbro, granite, and quartzite under axial compression. Q^{-1} remained constant as axial stress was increased up to 300 bars, then started decreasing with stress. However, Rao and Ramana (1974) found that in metamorphic rocks, Q^{-1} for axial P waves decreased as stress was increased to half the failure strength, then increased. Lockner et al (1977) explained these results as being due to changes in frictional dissipation on crack surfaces as the crack distribution is modified by the axial stress.

Effect of temperature. Volarovich and Gurvich (1957) and Kissel (1972) investigated the effect of temperature on attenuation in igneous and sedimentary rocks in air. Some of their results are shown in Fig. 1.3. Kissel (1972) found that Q^{-1} had a peak near room temperature and decreased at lower and higher temperatures. He observed that his samples lost 0.1% to 2% of their weight by heating to 600 °C. Volarovich and Gurvich (1957) only made measurements above room temperature, but they went to higher temperatures, up to 1000 °C. Q^{-1} was found to have a minimum near 300 °C and

Fig. 1.3. Variation of Q^{-1} with temperature. ▽ Barre granite (Kissel 1972); o Kutaisi basalt, □ gabbro, △ quartzite (all from Volarovich and Gurvich 1957).

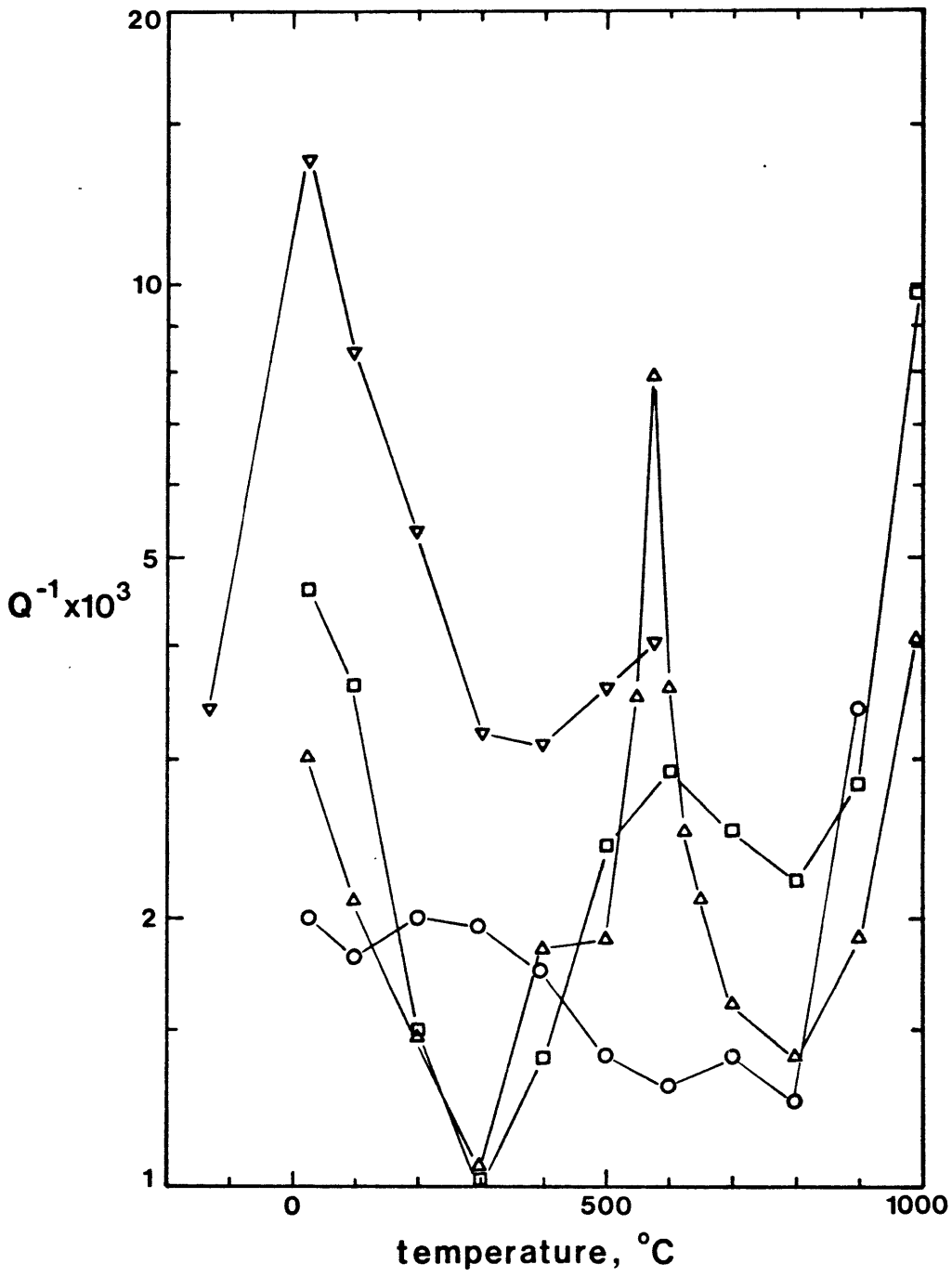
20
10
5
2
1
$Q^{-1}x10^3$
0
500
1000
temperature, °C

to increase at higher temperatures. Rocks containing quartz had a peak in Q^{-1} near the α-β quartz transition, 573 °C, especially the quartzites. Granites had a smaller peak near 600 °C and the diabases had no increase in Q^{-1} until 900 °C. Tittmann et al (1978) measured the attenuation of a basalt in a vacuum of 2×10^{-7} torr between -100 °C and 450 °C. They found a maximum Q^{-1} at 100 °C and a minimum at -100 °C.

Effect of amplitude. For rocks, Q^{-1} is independent of strain amplitude in the range 10^{-9} to 10^{-6}, but increases at higher strains (Gordon and Davis 1968, Winkler et al 1979). Winkler et al (1979) showed that the increase in Q^{-1} as strain amplitude is increased was approximately the same for room dry and saturated samples, but was much less for a sample dried in a vacuum oven.

1.4 Theory

In this section, attenuation mechanisms that may be important under laboratory and upper crustal conditions are summarized. Jackson and Anderson (1970) reviewed attenuation mechanisms that may be important in the earth's mantle.

The observations that Q^{-1} is independent of frequency in dry rocks have led to the postulation of friction between crack surfaces as the mechanism of attenuation, since the classic Coulomb friction, and therefore the energy dissipated by friction, are independent of the velocity of sliding of the surfaces. Walsh (1966) calculated the attenuation of P and S waves in rocks with random distributions of cracks

by approximating the cracks as thin elliptical voids in plane stress. As the stress wave passes, those cracks oriented so that the shear stress acting on them is greater than the frictional shear stress will slide and so dissipate energy. The attenuation depends on the friction coefficient and the crack density $\epsilon = N_v a^3$, where N_v is the number per unit volume of cracks of half-length a that are just in contact. For reasonable values of the friction coefficient his analysis gives a ratio of Q_S^{-1}/Q_P^{-1} between 0.4 and 1.0, which agrees with laboratory measurements, but the model requires rather high values of crack density. The friction mechanism and the arguments that have been made against it are considered in Chap. 2.

In a partially or fully saturated rock, motion of the fluid also causes attenuation. Two types of mechanism have been proposed. One is viscous shear relaxation in the fluid. Walsh (1969) analyzed this mechanism and concluded that it could be important at seismic frequencies for partial melt conditions in the upper mantle. For water in crustal rocks, viscous relaxation is probably important only at frequencies greater than 10^6 Hz. The second type of mechanism is flow between cracks, sometimes called squirt flow (Mavko and Nur 1975, O'Connell and Budiansky 1977). As a stress wave passes through a rock, cracks of different orientations with respect to the applied stress are deformed by different amounts. The resulting fluid pressure differences among cracks cause flow which dissipates

energy near the frequency at which the period of the wave is equal to the relaxation time τ_1 required for the flow. If the rock has a wide range of crack geometries, the attenuation can be spread over a broad range of frequencies. O'Connell and Budiansky (1977) give several estimates for the relaxation time, one of which is $\tau_1 = \eta/K\alpha^3$, where η is the fluid viscosity, K is the matrix bulk modulus, and α is the crack aspect ratio. For crack aspect ratios between 10^{-4} and 10^{-2}, this expression predicts that fluid flow attenuation is important between 10 and 10^6 Hz. Johnston et al (1979) derive a different expression for the relaxation time for flow between cracks and equant pores that predicts that fluid flow attenuation is important at frequencies of 10^3 and higher.

If the rock is not completely saturated the resistance to fluid flow from saturated cracks to empty cracks or pores is reduced and fluid flow losses should be enhanced. This situation has been analyzed from two points of view. Johnston (1978) considered the case of gas bubbles in a mostly saturated rock and Mavko and Nur (1979) considered fluid drops in cracks. The relaxation times depend on the shapes and sizes of the fluid drops or gas bubbles.

In addition to physical attenuation mechanisms, scattering of elastic waves can cause an apparent attenuation when the wavelength is similar to the size of the inhomogeneities in the rock. Scattering can be important in laboratory measurements at frequencies of 10^6 or higher,

when the wavelength is on the order of millimeters or less, comparable to the grain size of most rocks. Scattering may also be important in the earth at lower frequencies in regions where larger scale inhomogeneities occur.

Chapter 2

ATTENUATION DUE TO FRICTION IN CRACKS

2.1 Introduction

The mechanism of attenuation by friction on crack surfaces described by Walsh (1966) accounts for the observations that Q^{-1} is constant with respect to frequency over the range 10^{-3} to 10^{5} Hz in dry rocks. Two criticisms of this mechanism, considered in detail below, are: (i) that the number of cracks required to provide the measured attenuation is unreasonably high (Savage 1969), and (ii) that frictional attenuation should be amplitude dependent and since amplitude dependent Q^{-1} is found only at strains above 10^{-6}, friction is unimportant at the much lower strain levels of seismic waves in the earth (Mavko 1979, Winkler et al 1979). These criticisms are valid only for cracks that are completely dry, a condition that is unlikely to occur in the crust and does not occur in laboratory measurements of attenuation in rocks in normal atmosphere. In this chapter we present evidence that in most rocks there are significant numbers of very narrow cracks that are filled with water under room dry conditions. Therefore, the two criticisms are based on invalid assumptions and do not apply. We then extend Walsh's (1966) theory by including the concept

of boundary lubrication and show that the improved theory of attenuation due to friction in cracks lubricated with water is a reasonable mechanism for explaining attenuation in nominally dry rocks.

2.2 Summary of Walsh's model of attenuation in rock due to friction

The following is a summary of Walsh's (1966) analysis of attenuation in rock due to friction between crack surfaces in contact. The cracks are assumed to behave as thin elliptical cracks in plane stress and are assumed to be equidimensional in plan view. As a stress wave passes through the rock, sliding occurs between opposite crack faces in those cracks that are barely closed and are oriented so that the applied shear stress on the crack surfaces is greater than the frictional shear stress. Work done against friction is dissipated as heat, resulting in attenuation of the wave.

For a crack on which friction does occur, the energy dw dissipated due to an increase in applied stress is

$$dw = \left(\frac{2\pi a^3}{E}\right) \mu\sigma d(\tau - \mu\sigma) \qquad (2.1)$$

where

a = half-length of the crack

E = Young's modulus of the rock matrix

μ = coefficient of friction between the crack surfaces

σ = applied stress normal to the plane of the crack

τ = applied shear stress in the plane of the crack

The condition that sliding occurs is

$$|\tau| > \mu\sigma, \tag{2.2}$$

and for the crack to be closed,

$$\sigma > 0 \tag{2.3}$$

The total energy loss per cycle is found by integrating (2.1) for each crack and summing the result for cracks of all orientations which contribute to frictional dissipation, as defined by the bounds (2.2) and (2.3). When the integration is done for P and S waves, the expressions for Q^{-1} are too long to be presented conveniently in closed form, but they are plotted in Fig. 2.1. Q^{-1} depends on the density of barely closed cracks $\epsilon' = N_v a^3$; μ, the friction coefficient; $\bar{E}/E$, the ratio of effective to matrix Young's modulus of the rock; and $\bar{\nu}$, the effective Poisson's ratio of the rock. The crack density ϵ' refers only to those cracks contributing to friction (i.e., those barely closed in this analysis) and not to the total crack density.

2.3 Criticism of the frictional attenuation model

In more detail, the first criticism mentioned above is as follows (Savage 1969). Only cracks that are "barely closed" contribute to friction. A small hydrostatic pressure applied to the rock would clamp those cracks so that a small amplitude stress wave could not cause them to move and they would no longer contribute to frictional dissipation. A new set of cracks previously open and now barely closed would be

Fig. 2.1. Relationship between Q^{-1}, friction coefficient η, and material constants for longitudinal and transverse waves. $\overline{E}/E$ is the ratio of effective to intrinsic Young's modulus, ϵ' is the crack density contributing to friction, and $\overline{\nu}$ is the effective Poisson's ratio. From Walsh (1966).

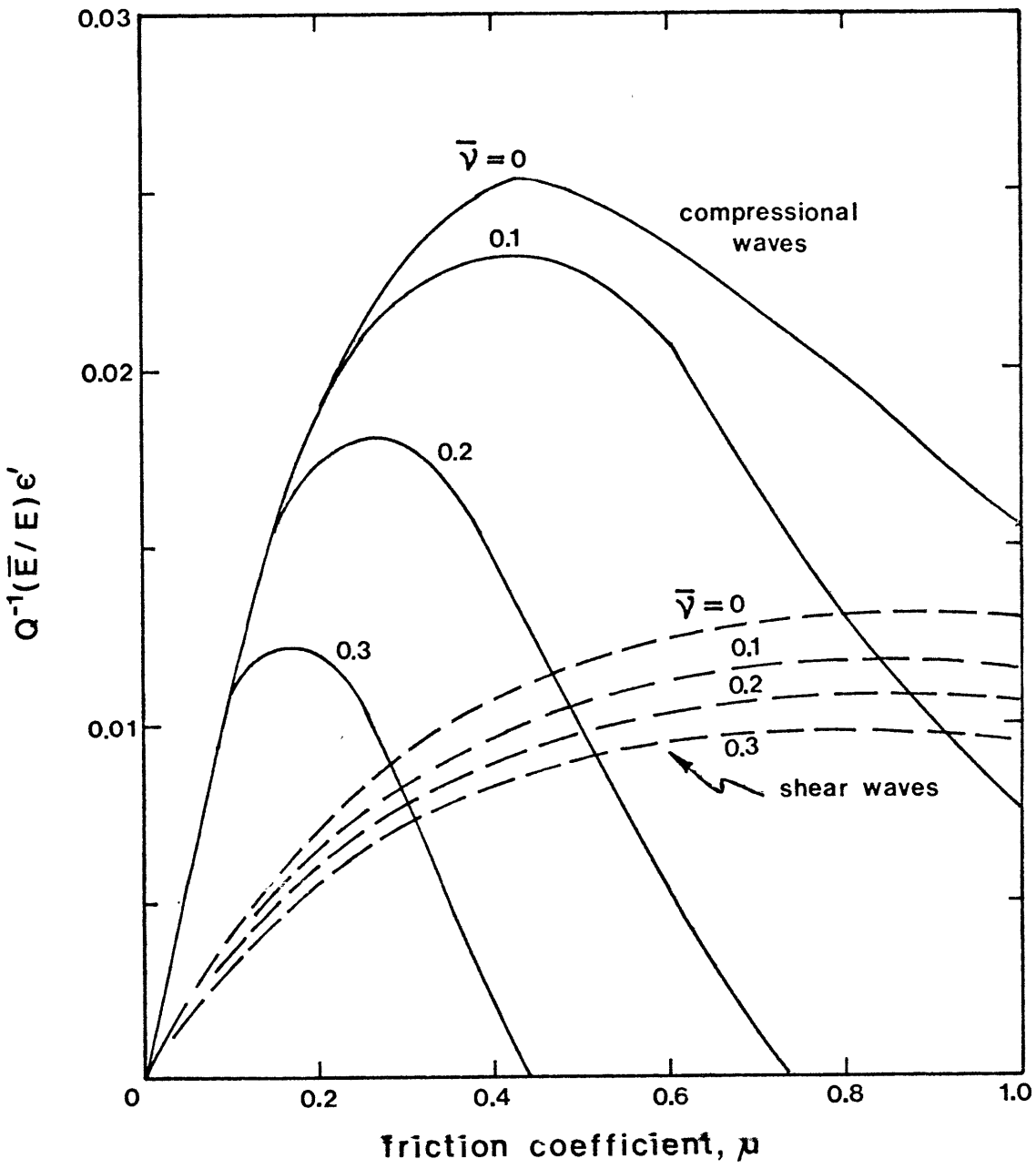
0.03
0.02
0.01
0
0.2
0.4
0.6
0.8
1.0
$Q^{-1}(\bar{E}/E)\epsilon'$
friction coefficient, μ
$\bar{\nu}=0$
0.1
0.2
0.3
compressional waves
$\bar{\nu}=0$
0.1
0.2
0.3
shear waves

required to account for the attenuation at this small hydrostatic pressure. Since cracked rocks have significant attenuation at pressures up to several hundred bars, on the basis of this argument, an extremely large number of sets of cracks would be required to account for the observed attenuation, each set being barely closed at a particular small increment of pressure. Since Walsh (1966) and Gordon and Davis (1968) showed that essentially all the cracks need to be contributing to explain the observed attenuation at zero confining pressure, Savage (1969) concluded that the frictional model required crack densities much higher than actually found in rocks and that friction therefore could not explain low-amplitude attenuation in rocks.

The second criticism is based on the analysis of frictional energy loss under combined normal and shear loading of spheres (Mindlin and Deresiewicz 1953) and of cracks with smooth surfaces and tapered ends (Mavko 1979). In both cases frictional energy loss is calculated to be proportional to the cube of the shear stress amplitude. Since the stored energy is proportional to the square of the stress amplitude, the resulting Q^{-1} is proportional to amplitude. Mavko (1979) generalized from these specific geometries and concluded that attenuation due to friction on crack surfaces is inherently amplitude dependent. In that case friction is unimportant for low amplitude seismic waves such as occur in the earth since amplitude-dependent Q^{-1} is observed in the laboratory only at strains greater than 10^{-6}.

Interestingly, experimental determinations of energy loss in shear between spheres in contact by Mindlin et al (1952) and Johnson (1955) showed that at low amplitudes energy loss was proportional to the square of the amplitude, i.e. Q^{-1} was independent of amplitude, and only at higher amplitudes was the energy loss proportional to the cube of the amplitude as predicted by theory. These observations cast doubt on the validity of the theory at low amplitudes and imply that friction may indeed produce an amplitude independent Q^{-1}.

Both criticisms are implicitly based on the assumptions that cracks in rocks are dry and that actual contact between opposite crack faces is required for friction to occur. Actually, because of the strong affinity of water for silicate surfaces, in normal atmosphere all cracks with widths less than 100 to 200 Å will be filled with water.

2.4 Occurrence of water in rocks

Two effects tend to hold water in the cracks in rocks: the adsorption of water on surfaces, and capillarity. The thickness of the adsorbed water layer depends on the temperature, humidity, and material. Holland (1964) reported measurements of the thickness of adsorbed water on glass wool determined by weight loss on heating, which are given in Table 2.1. The thickness of the adsorbed water was 105 Å at room temperature and decreased as temperature was raised. The measurements of several authors of water thickness at different relative humidities are given in Table 2.2. The

Table 2.1. Effect of temperature on adsorbed water thickness on glass wool. Thickness was determined by weight loss on heating. (from Holland 1964, p. 231)

temperature, °C	apparent H_2O thickness, Å
23	105
107	67
215	55
329	36
415	13
468	4
503	0 (reference)

Table 2.2. Effect of relative humidity on adsorbed water thickness. Frazer (1929), Hall (1970), and Tittmann et al (1977) used the ellipsometry method, in which the thickness of the surface film is estimated from its effect on the polarization of a beam of plane polarized light reflected near the Brewster angle. Hagymassy et al (1969) used the adsorption isotherm method.

reference	Frazer (1929)	Hagymassy et al (1969)	Hall (1970)	Tittmann et al (1977)
material	glass	quartz, fused silica	fused silica	basalt
p/p_s	apparent H_2O thickness, Å			
1.0		20	80	<60 (uneven coverage)
0.95	24	12	7	
0.9	20			
0.85		9		
0.6	6	6		
0.4	3			
0.05				<30

variability is probably due to differences in surface preparation, especially surface roughness. Perhaps the best values from the point of view of this discussion are the ones of Tittmann et al (1977), since they used a rock. We will thus assume that the thickness of the adsorbed water layer in cracks in rocks is between 30 and 60 Å. For comparison, a monolayer of water has a thickness of 3 Å.

As a result of the surface tension of a liquid, the vapour pressure is different over a curved liquid surface than over a plane surface. This effect is called capillarity. The vapour pressure is lower over a concave surface than a plane and therefore liquid condenses in narrow cracks and capillaries. In a humid atmosphere, water fills all cracks narrower than width $w = 2r_m \cos\theta_c + 2z$, where r_m is the equilibrium radius of curvature of the water-air interface at a given water vapour pressure, θ_c is the contact angle between water and the solid surface, and z is the thickness of the adsorbed water layer (see Fig. 2.2). For water on silicate surfaces, θ_c is approximately zero. The relation between r_m and the vapour pressure is called the Kelvin equation, which has been experimentally verified for r_m as small as 40 Å by Fisher and Israelachvili (1979):

$$\ln\left(\frac{p}{p_s}\right) = \left(\frac{M}{\rho RT}\right)\cdot\left(\frac{\gamma}{r_m} - (p - p_s)\right) \qquad (2.4)$$

where

p = vapour pressure

p_s = saturation vapour pressure

Fig. 2.2. Capillary and adsorbed water in a crack. Water will condense in cracks narrower than $w = 2r_m\cos\theta_c + 2z$, and will evaporated from wider cracks, where r_m is the mean radius of curvature of the water-air interface, θ_c is the contact angle between water and the crack surface and z is the adsorbed water thickness.

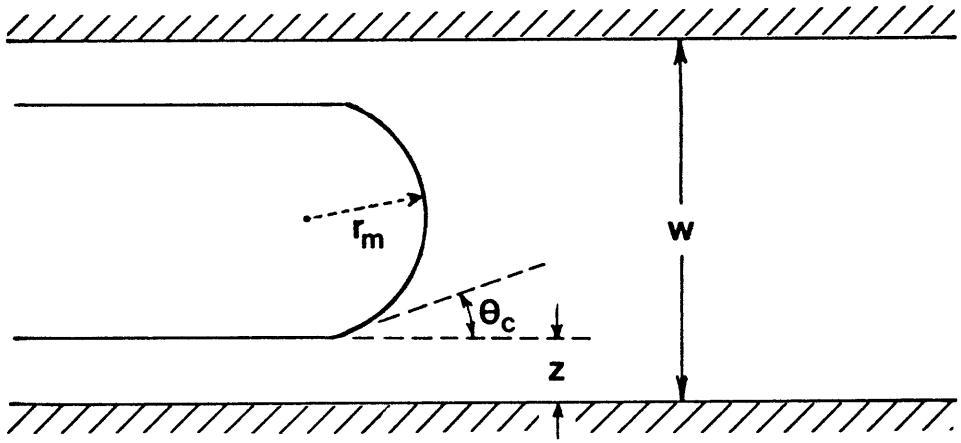
r_m
θ_c
z
w

M = molecular weight of the liquid

ρ = density of the liquid

R = gas constant

T = temperature, °K

γ = liquid-vapour interfacial tension

$\frac{1}{r_m} = \frac{1}{r_1} + \frac{1}{r_2}$ where r_1 and r_2 are the principal radii of curvature of the surface.

For a planar crack, r_2 is infinite (into the plane of Fig. 2.2), so $r_m = r_1$. For water, (2.4) gives r_m = 25 Å at 80% relative humidity, and r_m = 10 Å at 60% relative humidity.

Combining the results for capillary water and adsorbed water, water will fill those cracks in rocks that have widths less than 80 to 170 Å in normal atmosphere.

Densities of cracks less than 200 Å have not been measured, although such cracks must exist in rocks in the laboratory. Hadley (1976) measured numbers and sizes of cracks in Westerly granite using a scanning electron microscope. The width of visible cracks was limited by the thickness of the gold coating applied to the specimen, about 200 Å. However, approximately 1/8 of the cracks she counted had widths of 300 Å or less, suggesting that many cracks of smaller width exist. Such narrow cracks must also exist in order to account for the surface conduction contribution to electrical conductivity measurements (Madden 1976). The crack density ϵ that Hadley (1976) measured for cracks of width greater than 200 Å was 0.18. The total ϵ required

to account for the compressibility of Westerly is 0.35 (see Table 3.1). This value is a lower limit since the equations for dry rocks were used to calculate it. The narrow cracks we are interested in for friction are filled with water and cracks filled with water have a smaller effect on compressibility than empty cracks (Kuster and Toksoz 1974, Budiansky and O'Connell 1976). Therefore, the ϵ of thin cracks, that is, those contributing to frictional dissipation, could be 0.17 or higher, if the area chosen for counting was representative of the whole rock and the uncertainty in relating the measured dimensions of cracks to the parameter ϵ determined from a theoretical model is not too large. For a friction coefficient of 0.2 to 1.0, Walsh (1966) gives Q^{-1} for shear waves as (see Fig. 2.1)

$$Q_S^{-1} \simeq 0.01(\bar{E}/E)\epsilon \qquad (2.5)$$

where $\bar{E}/E$ is the ratio of effective to intrinsic Young's modulus. For Westerly granite $\bar{E}/E$ is 0.67 (Simmons and Brace 1965). The Q^{-1} of room dry Westerly is 5.7×10^{-3} (Table 4.1). Using these values in (2.5) gives a crack density of 0.85, or 5 times too high. The discrepancy may be because (i) the density of narrow cracks is underestimated because they are filled with water, as mentioned above, or (ii) as Walsh (1966) suggested, actual cracks are connected and therefore less stiff than the isolated elliptical cracks used in the derivation of (2.5). Sliding displacements and therefore frictional dissipation in the real rock would be

greater than in the model, thus requiring a smaller crack density than the prediction.

2.5 Boundary Lubrication

Friction between surfaces separated by thin films, termed boundary lubrication, was reviewed by Ling et al (1969). In boundary lubrication a small fraction of the load is supported by solid-solid contacts, but most of the load is supported by the boundary film, which may be an oxide layer or a thin film of lubricant (in this case, water). Friction arises from the shearing of both the solid contacts and the boundary film. Measured friction coefficients are in the range 0.1 to 1.0, and depend on the composition of the solid, surface finish, lubricant, and interaction between the lubricant and the solid, but not on the bulk viscosity of the lubricant. Although most friction research is done at high loads and high speeds, a Coulomb friction law has been shown to be valid at small loads, from 10^{-5} to 10^{-2} gram (Whitehead 1950, Bowden and Tabor 1964); at low speeds, down to 10^{-6} cm/sec over displacements as small as 10^{-5} cm, much smaller than an average asperity contact size of the surfaces used (Heymann et al 1955).

Bowden and Tabor (1964) proposed that boundary lubrication could be described by the equation

$$F = S[\alpha s_s + (1 - \alpha) s_l] \tag{2.6}$$

where

F = frictional force

S = area of real contact (not the same as the apparent contact area)

a = fraction of S consisting of solid to solid contacts

s_s = shear strength of solid junctions

s_l = shear strength of boundary lubricant film

For materials that can deform plastically, such as metals, the area of real contact is

$$S = \frac{W}{P} \tag{2.7}$$

where W is the load and P is the yield stress of the contact asperities. Brittle materials obey (2.7) approximately (Tabor 1975). Under the local conditions that exist at the contacts of asperities, the stress field includes a large hydrostatic component which in many cases is sufficient to inhibit brittle failure and the asperities deform in a plastic manner, although some cracking may also occur. From the definition of the coefficient of friction and (2.6) and (2.7) we obtain

$$\mu = \frac{F}{P} = \frac{1}{P}[as_s + (1 - a)s_l] \tag{2.8}$$

If the ratios s_s/P and s_l/P are denoted by μ_s and μ_l, then

$$\mu = a\mu_s + (1 - a)\mu_l \tag{2.9}$$

where μ_s is the dry friction coefficient and μ_l is the friction coefficient when $a = 0$, that is, in the absence of true solid contact. Bailey and Courtney-Pratt (1955) measured the friction force between sheets of mica and measured the true contact area by optical interferometry.

They determined that the shear strength of an unlubricated mica contact was 1 kb and that the shear strength of the contact between mica sheets each covered by a single monolayer of calcium stearate was 25 bars, or one fortieth as large. The shear strength of six monolayers of calcium stearate was still lower. The experiments were carried out in atmosphere a brief time after cleavage of the mica sheets, so it is likely that in the unlubricated case the mica surfaces were covered by at least a monolayer of water. They thus demonstrated that thin lubricant films have significant shear strength, explaining why a boundary lubricant reduces the coefficient of friction only a factor of 10 while decreasing wear by a factor of up to 10^4 or more. Tamai and Rightmire (1965) showed that (2.9) was consistent with the differences in friction coefficient between fresh copper surfaces and copper surfaces with two different thicknesses of oxide. For twelve lubricants, μ_l/μ_s, or s_l/s_s ranged from 0.02 to 0.06; the larger values of μ_l were found for the lubricants with the more complicated molecular structures. The calculated values of α ranged from 0 to 3% for lubricants with dipole moments between 1.7 and 3.1 debye and was 23% for a non-polar liquid. For comparison, the dipole moment of water is 1.87 debye. Other studies have also shown that for a good lubricant α is a few percent or less (Bowden and Tabor 1964). A good lubricant is one that forms a continuous film separating the solid

surfaces and has strong lateral adhesion so that it resists penetration by asperities of the solid surfaces during sliding. Water is a polar liquid and is strongly bound to silicate surfaces, so that it should be a good lubricant for silicate minerals, although we do not know of any experiments for which s_l or a for water has been determined. If, however, in the experiments of Bailey and Courtney-Pratt (1955) it is true that in the unlubricated case a monolayer or more of water covered the mica surfaces, their results indicate that very thin water films have significant shear strength.

The important points of this discussion of boundary lubrication are that (i) most of the friction force is due to the shearing of the boundary lubricant film, and not to the shearing of actual solid contacts, and (ii) the coefficient of friction is in the range 0.1 to 1.0.

2.6 A model of attenuation based on friction in cracks lubricated with water

With the understanding that the cracks contributing to frictional dissipation are not those that are barely closed but instead narrow cracks filled with water in which friction occurs by boundary lubrication, the analysis of Walsh (1966), summarized in Sec. 2.2, can be used for an improved model of attenuation in nominally dry rocks, in which the crack density ϵ' now refers to the density of narrow cracks lubricated by water. This improved model of frictional attenuation can be used to account for the

observed effects of hydrostatic pressure and strain amplitude on Q^{-1}, thus obviating the two criticisms given in Sec. 2.3, and can also account for the effects of temperature and high vacuum. As hydrostatic pressure is increased, the rough surfaces of the cracks are pressed together. As more asperities come into contact the crack becomes stiffer (Walsh and Grosenbaugh 1979), and the sliding displacement due to an applied stress wave decreases. Therefore, the frictional dissipation on each crack surface decreases. It is not necessary for the rock to contain many different sets of cracks that become barely closed at successive increments of pressure. The same cracks contribute to frictional dissipation at all pressures, but each crack contributes less as pressure is increased and the cracks become stiffer.

Two processes may contribute to the amplitude dependence of Q^{-1} at strains greater than 10^{-6}:

1. For a shear modulus of 0.2 Mb (Westerly granite, Simmons and Brace 1965) a shear strain of 10^{-6} corresponds to a stress of 0.2 bar. At smaller stresses there is probably negligible deformation of asperity contacts between crack surfaces, relatively few asperities are in actual contact, and Q^{-1} is constant. At higher stresses more asperities come into contact and the attenuation due to friction at these contacts may be amplitude dependent as predicted by contact theory.

2. At strains higher than 10^{-6}, crack surfaces which at

lower strains were not contributing to friction may be closed sufficiently for their adsorbed water layers to come into contact and so increase the number of cracks on which frictional dissipation occurs; thus Q^{-1} would increase.

As temperature rises or the water vapour pressure decreases, the thickness of the adsorbed water layer on crack surfaces decreases (Tables 2.1 and 2.2). Simmons (personal communication) has shown that water is driven off by heating a rock up to 200 °C. As the thickness of the adsorbed water layers is decreased, the crack surface area contributing to friction is reduced as some cracks previously saturated are no longer bridged by water films. As the crack area contributing to friction decreases, Q^{-1} decreases.

2.7 Summary

This chapter can be summarized as follows. Cracks in rocks contain adsorbed and capillary water. Frictional dissipation thus occurs over large areas of crack surfaces and not only the small fractional area of actual asperity contact. Friction on crack surfaces lubricated by thin films of water can account for the observed attenuation in nominally dry rocks and the effects of pressure, strain amplitude, temperature, and vacuum on attenuation.

The friction mechanism has been discussed in this chapter as applied to nominally dry rocks. The data presented in Fig. 1.1 show that for a broad frequency range attenuation due to fluid flow is more important than friction in laboratory measurements on saturated rocks. However, in the crust

of the earth as depth increases, lithostatic confining pressure tends to close cracks, so that it is likely that microcracks in the crust are narrower in general than the cracks in rocks collected at the surface. As the cracks become narrower, a larger proportion of them contribute to frictional dissipation. In addition, since the water in very narrow cracks is mostly adsorbed water and thus bound to the crack surfaces, fluid flow becomes less important. Therefore, we believe that in the crust, friction is an important attenuation mechanism, and may in fact be the dominant attenuation mechanism, even under saturated conditions.

Chapter 3

MATERIALS AND PROCEDURES

3.1 Samples

The samples used in this study are mainly Precambrian igneous rocks from central Wisconsin and southeast Missouri. Also included are Westerly and Chelmsford granites and Frederick and Pageland diabases. Locations and selected physical properties of the rocks are given in Table 3.1 and their modal compositions are given in Table 3.2.

3.2 Apparatus

Attenuation was measured with a torsional pendulum shown schematically in Fig. 3.1, that was also used by Jackson (1969). The flywheel has a mass of 50 kg and is suspended from the ceiling. The sample is attached to the flywheel and to the base by face-plate collett chucks.

The optical system used to measure the rotation of the flywheel is shown schematically in Fig. 3.2. A beam of light is reflected by a mirror on the flywheel onto a beam splitting lens. The outputs of the two phototubes are subtracted and the result amplified and plotted by a chart recorder. The sensitivity of the recording system is approximately 120 volts per radian and it is possible to measure oscillation amplitudes as small as 10^{-5} radians, the

Table 3.1. Sample locations and physical properties. Crack porosities for samples 1242, 1331, 1336, 1343, 1368, 1370, 1407, 1409, 1410, 1411, and 1415 were published in Feves et al (1977). Crack porosities for the other rocks were determined from DSA data collected by M. L. Batzle, M. Feves, and H. W. Cooper. Compressibilities were determined from the same DSA data as the crack porosities. Crack densities were calculated from the compressibilities by the method described in Sec. 5.1.

sample #	name	location	crack porosity x 10^6	compressibility, Mb^{-1}		crack density
				β(0 kb)	β(2 kb)	ϵ
A757	granite	Chelmsford, Ma	2370	9.92	2.09	0.39
806	granite	Westerly, RI	1450	7.67	2.08	0.35
812	diabase	Pageland, SC	25	1.37	1.28	0.02
1242	diabase	Frederick, Md	<5	1.30	1.30	0.00
1328	gabbro	Hurley, Wi	805	3.52	1.81	0.18
1331	gabbro	Mellen, Wi	70	1.44	1.24	0.04
1336	granite	Wausau, Wi	370	2.86	2.02	0.12
1343	granite	Wausau, Wi	860	5.14	1.85	0.29
1368	gabbro	Tigerton, Wi	60	1.50	1.40	0.02
1370	quartz monzonite	Red River, Wi	830	3.98	2.10	0.20
1381	gabbroic anorthosite	Mellen, Wi	190	1.46	1.08	0.09
1401	diabase	Fredericktown, Mo	75	1.62	1.46	0.03
1403	felsite	Fredericktown, Mo	185	2.36	2.02	0.05
1407	felsite	Middlebrook, Mo	155	1.67	1.49	0.04
1409	granite	Graniteville, Mo	885	4.42	2.45	0.19
1410	granite	Graniteville, Mo	615	3.68	2.24	0.16
1411	rhyolite	Stouts Creek, Mo	605	3.18	2.05	0.14
1415	diabase	Skrainka, Mo	<5	1.33	1.29	0.01

Table 3.2. Modal analysis. Modal compositions are not available for samples 1328, 1381, 1401, and 1403.

sample #	A757	1134[a]	812	890[b]	1331	1336	1343	1368	1370	1407	1409	1410	1411	1415
plagioclase	28.5	39.2	63.7	47.3	53.7	23.8	10.0	52.0	33.7	0.3	29.3	26.9	16.1	66.9
K feldspar	34.8	30.7				44.8[d]	49.6[d]		25.7[e]		30.4[d]	39.3[d]		
quartz	30.1	22.5				28.9	39.1		28.5	6.7	39.8	32.8	8.3	
pyroxene			29.2	46.9	30.1			24.3	0.9					8.8
olivene			2.0	0.4	1.1			0.3						14.2
biotite	2.1	5.0		0.8			tr	18.0	9.5					2.3
opaque	0.1	0.9	1.1	2.5	3.1	1.0	tr	4.1	0.7		tr	tr	0.4	4.7
secondary	1.2	0.4	4.0	2.2	12.2	1.5	0.8	1.1	0.3	1.0	tr	0.5	2.5	3.1
matrix[c]										77.5			72.7	
others	3.1	1.3				tr	0.3	0.2	0.7	14.5	0.5	tr		
total	99.9	100.0	100.0	100.1	100.2	100.0	99.8	100.0	100.0	100.0	100.0	99.5	100.0	100.0
number of counts	2730	1000	1000	2413	1002	1000	1200	1000	1000	1000	1000	1200	1000	1000
avg. grain size, mm	1.5	0.8	0.6	0.5	0.6	1.0	2.0	0.6	0.8	<0.1	1.0	0.9	0.4	1.2
reference for mode	f	g	h	g	g	g	g	g	g	g	g	g	g	g
ref. for petrographic description	i	j	k		l		l	l	l	l		l	l	l

see next page for footnotes

Table 3.2 continued

tr denotes trace

[a]The mode given for Westerly granite is for sample 1134. Sample 806 was used for the physical property measurements of Table 3.1. These two samples were collected at different times from the same locality and have similar properties.

[b]The mode given for Frederick diabase is for sample 890. Sample 1242 was used for the physical property measurements of Table 3.1. These two samples were collected at different times from the same locality and have similar properties.

[c]fine grained quartz and feldspar matrix.

[d]perthite.

[e]microcline.

[f]Cooper and Simmons (1977)

[g]Feves *et al* (1977)

[h]Simmons and Cooper (1978)

[i]Dale (1923)

[j]Fairbairn *et al* (1951)

[k]Raglan *et al* (1968)

[l]Richter and Simmons (1977)

Fig. 3.1. Schematic of the apparatus. After Jackson (1969)

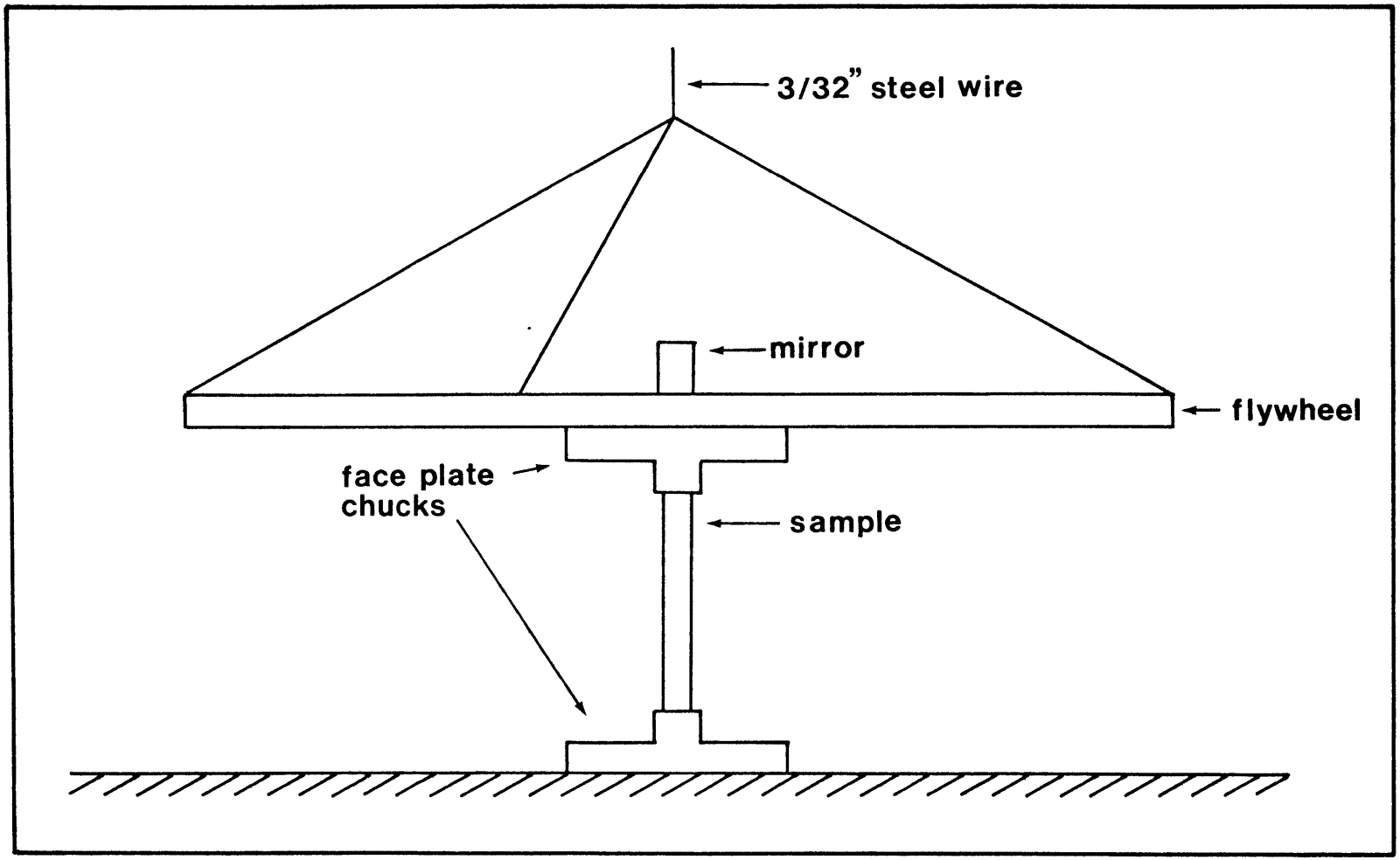
3/32" steel wire
mirror
flywheel
face plate
chucks
sample

Fig. 3.2. Schematic of the recording system. From Jackson (1969).

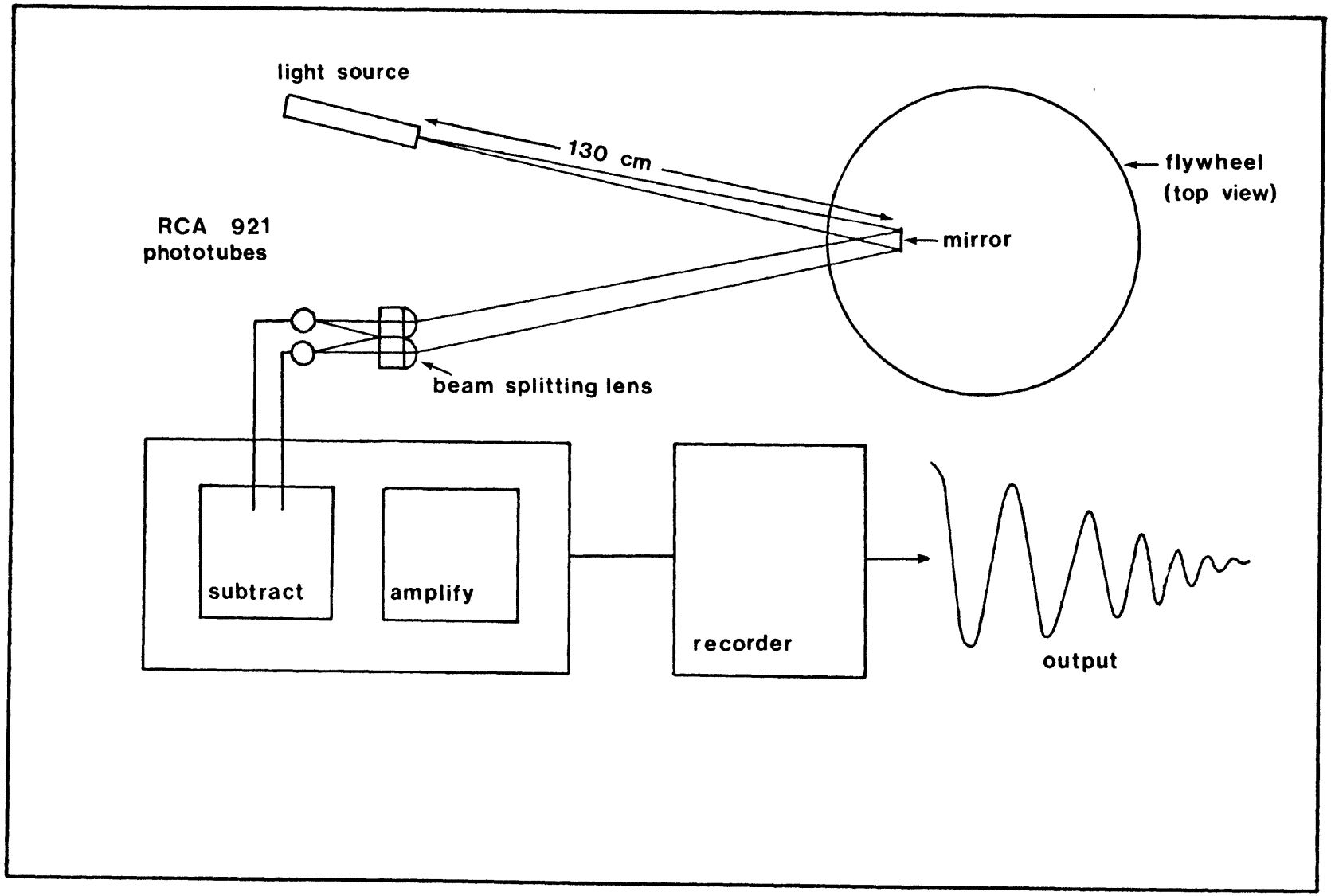
light source
130 cm
flywheel
(top view)
RCA 921
phototubes
mirror
beam splitting lens
subtract
amplify
recorder
output

noise level of the system. The strain at the surface of the sample is $a\theta/L$ where a is the sample radius, L is the sample length, and θ is the angle of rotation, so that oscillations at sample strains of 10^{-6} or less can be measured, for samples of radius to length ratio of 0.1 or less.

The equation of motion of an ideal torsional pendulum is

$$J\frac{d^2\theta}{dt^2} + K\theta = 0 \tag{3.1}$$

where

J = moment of inertia of the flywheel

K = stiffness of the shaft = $(\pi/2)Ga^4/L$

G = shear modulus of the shaft

a = shaft radius

L = shaft length

θ = angle of rotation

A solution of the form $\theta = A\cos(\omega t)$ where A is the amplitude of the oscillation and ω is the angular frequency, requires that

$$-\omega^2 JA + KA = 0 \tag{3.2}$$

Therefore,

$$\omega^2 = \frac{K}{J} = \frac{\pi G a^4}{2JL} \tag{3.3}$$

Since $\omega = 2\pi f$, the frequency of oscillation f is given by

$$f = \left(\frac{Ga^4}{8\pi JL}\right)^{1/2} \tag{3.4}$$

The moment of inertia of the flywheel was determined from aluminum standards to be 1.6×10^7 g cm^2.

Since f varies as a^2, the frequency of oscillation can be varied most easily by using samples of different radii. A practical range of frequencies was found to be from about 0.5 Hz for samples 0.5 cm diameter and 20 cm long to about 3 Hz for samples 1.2 cm diameter and 10 cm long. Samples thinner than 0.5 cm diameter were too fragile for easy handling with this equipment. At frequencies above 3 Hz, since the strain also depends on sample radius, it was not possible to accurately measure attenuation at strains low enough to be in the constant Q^{-1} range.

3.3 Procedures

The procedure used to calculate Q^{-1} was to measure the amplitude A at a number of times on the strip chart, plot lnA versus time and then fit in the least squares sense a straight line to the low amplitude portion of the points where the slope was constant. Then

$$Q^{-1} = \frac{1}{\pi f} \frac{d\ln A}{dt} \tag{3.5}$$

At strains higher than approximately 5×10^{-6}, dlnA/dt was found not to be constant. In that case, Q^{-1} can be calculated as a function of strain amplitude using the following equation, derived in Appendix B:

$$Q^{-1}\left(\frac{aA}{L}\right) = \frac{1}{\pi f} \frac{d\ln A}{dt} + \frac{1}{4\pi f}\left(\frac{d\ln A}{dt}\right)^{-1}\left(\frac{d^2 \ln A}{dt^2}\right) \tag{3.6}$$

Measurements were made under conditions called room dry and saturated. For room dry conditions, cores were evacuated at 10^{-2} torr for at least 72 hours to remove

residual free water, then the samples were exposed to laboratory air for at least 72 hours to assure equilibration at laboratory humidity. As explained previously the term room dry does not imply that the cores are completely dry. The various cores do not necessarily have the same degree of saturation nor is the saturation in a single core necessarily homogeneous since that depends on the widths of the cracks. The cores were saturated by evacuating them to 10^{-2} torr pressure, then filling the vacuum chamber with distilled water. It is probably not possible to fully saturate a rock without applying some pore fluid pressure to dissolve residual air, so the saturation of the samples is estimated to be between 95 and 100%. The sample to be measured was kept saturated during the time needed to mount it in the equipment and to stabilize the electronics; it was wrapped in a wet cloth and then unwrapped just before the measurement was made. The surface of the sample would stay wet (as judged from visual appearance) long enough for the measurement of Q^{-1} to be made. Analysis of the data proved this simple procedure sufficient. If the degree of saturation of the sample had decreased during the measurement, then Q^{-1} would have changed with time and a constant rate of decay of lnA would not have been observed. In fact, for all saturated cores a constant value was obtained.

Measurements of Q^{-1} at elevated temperatures were made with a ceramic tube furnace around the sample, as shown in Fig. 3.3. Jackson (1969) used this arrangement for

Fig. 3.3. Schematic of the furnace and sample arrangement for attenuation measurements at elevated temperatures.

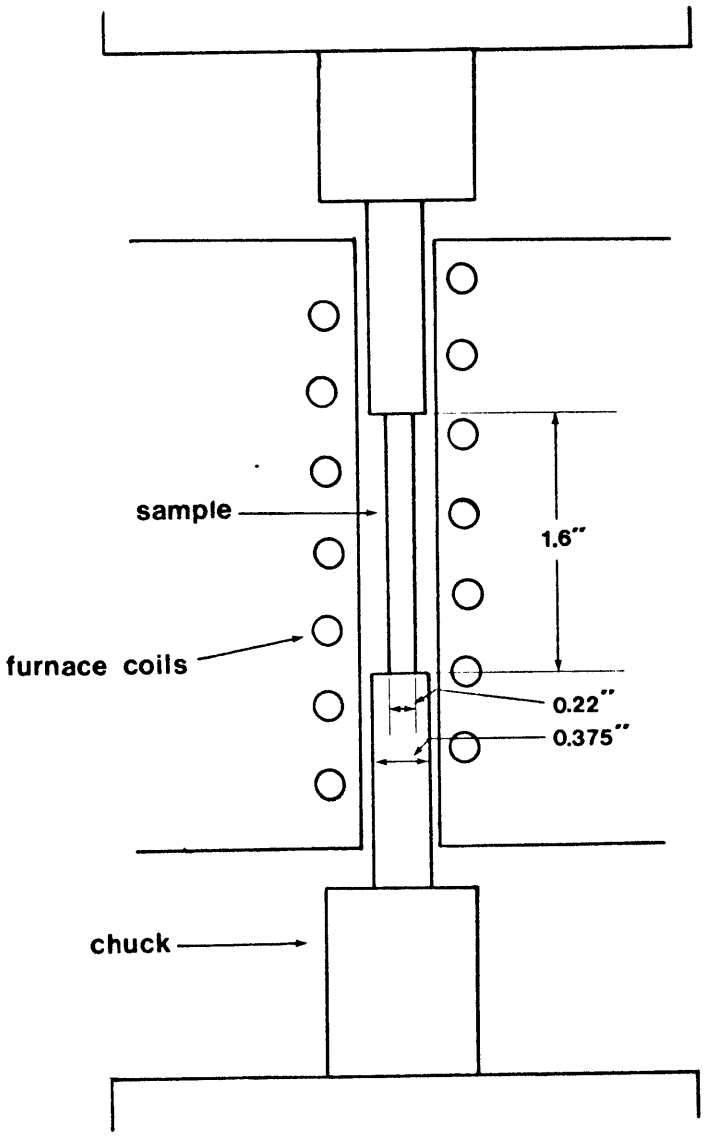
sample
furnace coils
chuck
1.6"
0.22"
0.375"

measuring attenuation of polycrystalline alumina, mullite, and forsterite. To concentrate the strain energy in that part of the sample in the center of the furnace, where the temperature in nearly uniform, he used samples ground into "dogbone" shapes, that is, with a central piece of smaller diameter than the ends. Because the central piece is of smaller diameter it is less stiff than the ends and most of the twist of the sample is concentrated there. Rock samples are not as strong as the ceramics Jackson (1969) used and tend to break at the point where the diameter of the sample changes, so a different sample arrangement was used in this study. Instead of dogbones ground from a core sample, the same geometry was obtained by using samples 0.22" diameter held in brass ends of 0.375" diameter by set screws. For the diameters of sample and end pieces, a sample length of 1.6" was used so that at least 90% of the strain energy would be in the sample. Using a longer work zone than Jackson (1969) did meant that temperature variations along the sample were greater than for his measurements. Three temperature profiles are shown in Fig. 3.4. The temperatures reported in Sec. 4.4 are mean values along the sample. At low mean temperatures, temperature variation along the sample is not very great, but at high temperatures the variation along the sample is so great that the mean temperature is not very meaningful. For the top curve in Fig. 3.4, the temperature difference between the middle and the ends of the sample is 140 °C. For that reason, temperatures above 350 °C in

Fig. 3.4. Temperature profiles in the furnace.

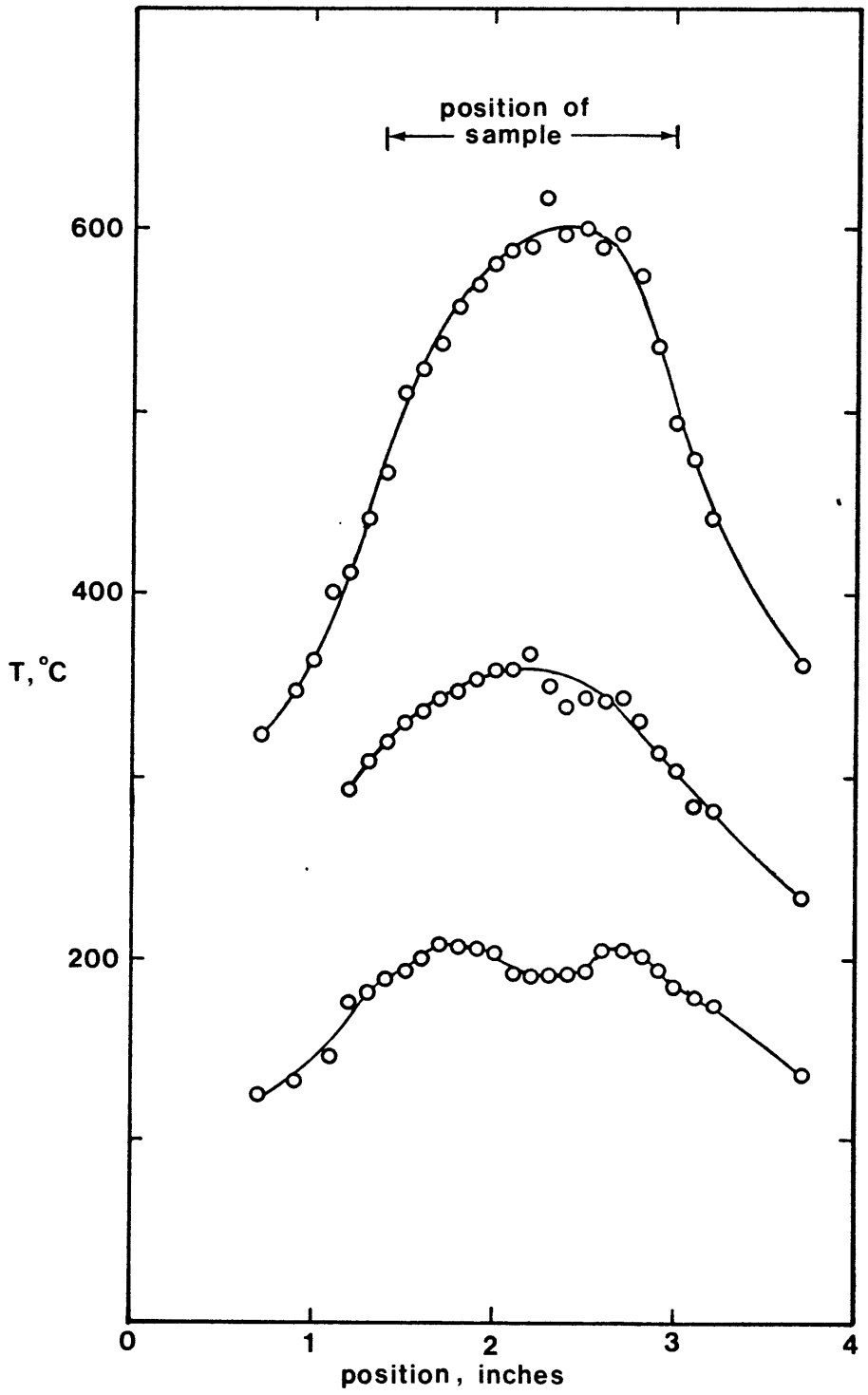
position of
sample
600
400
200
T, °C
0
1
2
3
4
position, inches

Sec. 4.4 must be regarded as being very approximate.

3.4 Error analysis

The procedure for the measurement of attenuation as described above will be valid provided that (i) all energy loss is due to the anelasticity of the sample and not due to losses in the sample clamping assemblies, the suspension of the flywheel, or air resistance of the flywheel; (ii) that all the elastic energy of the pendulum is stored in the sample, and none in the rest of the system; and (iii) that other modes of vibration are not excited. Measurements on samples of three low-loss materials, aluminum, brass, and fused silica gave a value of Q^{-1} of 3.3×10^{-4}. The actual values of Q^{-1} of these materials are not known at 1 Hz, but the measured value is probably due to system losses since (i) it is unlikely that three different materials would have the same Q^{-1} at 1 Hz and (ii) aluminum has a Q^{-1} of less than 10^{-5} between 840 Hz and 102 kHz (Zemanek and Rudnick 1961). Measurements of attenuation of rock samples were corrected for the system losses by subtracting this value of 3.3×10^{-4} from the measured Q^{-1}. For most samples the correction was less than 10%. Jackson (1969) stated that he designed the system so that at 1 Hz the elastic energy stored in the flywheel and suspension wire is less than 2×10^{-5} of the energy stored in the sample, and so that unwanted modes are energetically unfavorable compared to the torsional mode and thus are not excited.

The uncertainty in an individual measurement of Q^{-1} can be estimated in two ways:

1. From the differences in Q^{-1} measured on different cores from one block of rock. This estimate will include the effect of sample variability. Table 4.4 gives measured values of Q^{-1} of several cores in each of three orthogonal directions in Westerly and Chelmsford granites. The standard deviation of Q^{-1} from the mean for the samples in the same direction is 5.3% for the Westerly samples and 10.3% for the Chelmsford samples, or 8.1% for the combined data.

2. From the change in Q^{-1} on repeated measurements of one sample. Six cores of Chelmsford granite were measured twice under room dry conditions, as shown in Table 4.4. Each sample was first measured dry, then saturated and measured again, and then dried once more and Q^{-1} remeasured in the room dry condition. The changes in Q^{-1} range from -9.5% to +22.7%. The standard deviation of Q^{-1} calculated from the differences from the mean of the two measurements of each core is 8.8%.

The two estimates agree closely. We will use a value of ±10% as an estimate of the uncertainty of a measurement of Q^{-1}.

Chapter 4

RESULTS

4.1 Attenuation in eighteen igneous rocks

Room dry and saturated values of Q^{-1} for the rocks described in Sec. 3.1 are given in Table 4.1. The measurements were made at frequencies between 0.5 and 3.5 Hz. The data are plotted against the crack porosity of the rocks in Fig. 4.1 Q^{-1} varies from 8.8×10^{-4} to 7.6×10^{-3} for the room dry rocks and from 9.1×10^{-4} to 2.3×10^{-2} for the saturated rocks. For both dry and saturated cases, there is an increase in Q^{-1} with increasing crack porosity, but the amount of scatter about the general trend is greater than the estimated uncertainty of ±10% in each measurement. The upper dashed line in Fig. 4.1 is a least squares straight line fit between $\log(Q^{-1})$ and log(crack porosity) for the saturated rocks. It has a slope of 0.47 with a correlation coefficient of 0.93. The equation of the line is

$$\log(Q^{-1}) = -0.53 + 0.47 \log(\eta_c) \qquad (4.1)$$

where η_c is the crack porosity. The standard deviation of Q^{-1} from the line is 40%. The lower dashed line in Fig. 4.1 is a least squares line for the dry Q^{-1} values except for the three points for the lowest crack porosities. These

Table 4.1. Attenuation of dry and saturated rocks. Crack porosities were determined from DSA measurements; sources given in Table 3.1.

sample #	crack porosity $\times 10^6$	$Q^{-1} \times 10^3$	
		dry	saturated
A757	2370	8.1	19.5
806	1450	5.7	17.1
812	25	2.6	3.0
1242	<5	0.91	1.4
1328	805	4.0	
1331	70	1.3	2.2
1336	370	3.2	7.8
1343	860	3.4	8.9
1368	60	1.8	3.8
1370	830	5.2	15.3
1381	190	2.3	6.5
1401	75	2.2	
1403	185	1.1	3.0
1407	155	2.1	2.4
1409	855	6.6	17.5
1410	615	6.6	
1411	605	5.3	7.1
1415	<5	0.88	0.91

Fig. 4.1. Q^{-1} of dry and saturated rocks. See Table 4.1 for the data. The measurements were made at frequencies between 0.5 and 3.5 Hz.

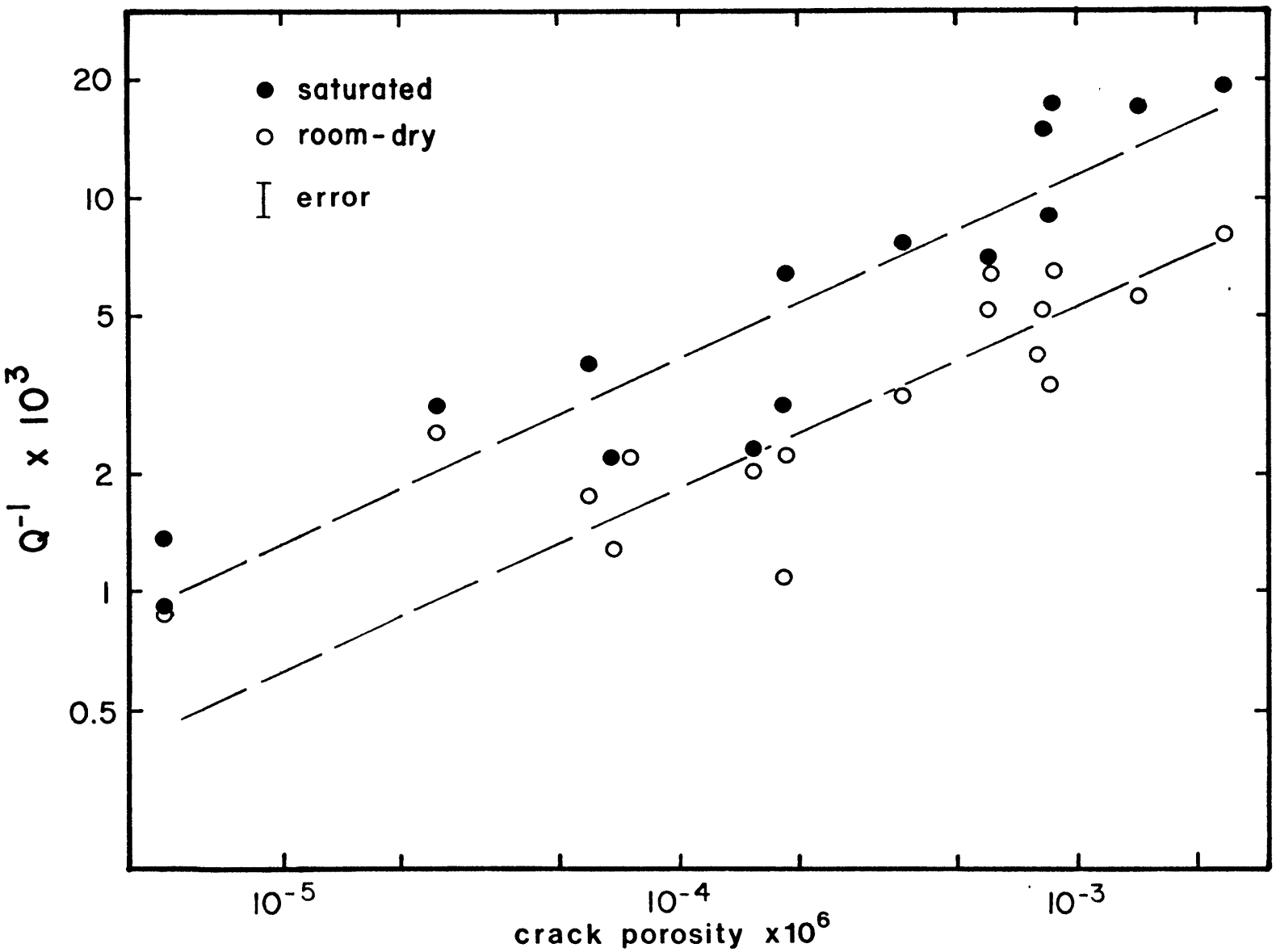
saturated
room-dry
error
20
10
5
2
1
0.5
$Q^{-1} \times 10^3$
10^{-5}
10^{-4}
10^{-3}
crack porosity $x10^6$

three points fall on the trend for saturated samples rather than dry, an observation from which we infer that they were not dried properly. The line through the rest of the points has a slope of 0.47 and a correlation coefficient of 0.87. Its equation is

$$\log(Q^{-1}) = -0.87 + 0.47 \log(\eta_c) \quad (4.2)$$

The standard deviation of Q^{-1} from the line is 30%. The slope of the regression lines is approximately 1/2 on a log-log plot which means that Q^{-1} is approximately proportional to the square root of the crack porosity. Q^{-1} of the saturated samples averages 2.3 times Q^{-1} of the dry samples (if we neglect the three samples with lowest crack porosity). If we set the slope of the lines at exactly 1/2, the equations of the regression lines become: (i) room dry:

$$\log(Q^{-1}) = -0.77 + 0.5 \log(\eta_c) \quad (4.3)$$

or,

$$Q^{-1} = 0.17\sqrt{\eta_c} \quad (4.4)$$

(ii) saturated:

$$\log(Q^{-1}) = -0.41 + 0.5 \log(\eta_c) \quad (4.5)$$

or,

$$Q^{-1} = 0.39\sqrt{\eta_c} \quad (4.6)$$

4.2 Attenuation in thermally cycled rocks

Thermal cycling, the slow heating and cooling of rocks, was used to produce known amounts of crack porosity in samples of Westerly granite and Frederick diabase (see

Simmons and Cooper 1978). Attenuation was measured on the thermally cycled samples with the hope that using samples of one rock that vary only in crack porosity would reduce the scatter observed in Fig. 4.1. The results, however, were different from those of Fig. 4.1.

Q^{-1} of thermally cycled Westerly granite is given in Table 4.2 and Fig. 4.2. There is no significant variation in room dry Q^{-1} as crack porosity increases. For the saturated samples, Q^{-1} decreases as crack porosity increases, opposite to the trend observed in Sec. 4.1.

Q^{-1} of thermally cycled Frederick diabase is given in Table 4.3 and Fig. 4.3. The maximum crack porosity produced in this set of samples is only 1/3 of the crack porosity of Westerly granite before thermal cycling. For the dry case Q^{-1} remains essentially constant up to a crack porosity of 250×10^{-6} and then increases. For the saturated samples, Q^{-1} also increases rapidly at crack porosities above 250×10^{-6}.

4.3 Anisotropy of attenuation

Anisotropy of attenuation was investigated in two rocks with anisotropic crack distributions, Westerly and Chelmsford granites. The Q^{-1} of dry and saturated cores cut with their axes in the rift, grain, and hardway directions of both rocks are given in Table 4.4. Also given is the differential strain analysis parameter ζ (Simmons et al 1974, Siegfried and Simmons 1978). ζ is the linear strai

Table 4.2. Attenuation of thermally cycled Westerly granite. Sample number is 806. Axes of the cores are in the hardway direction. Crack porosities were not measured on these samples, but were calculated from the maximum cycling temperature according to the relation found by Simmons and Cooper (1978).

maximum cycling temperature, °C	crack porosity x 10^6 (±25%)	Q^{-1} x 10^3 dry	Q^{-1} x 10^3 saturated
25	1450	5.1	14.0
130	2480	6.1	13.8
229	4100	5.3	11.4
326	6800	5.4	10.2
433	11,700	5.6	10.1
486	15,300	6.3	8.3

Fig. 4.2. Q^{-1} of thermally cycled Westerly granite. See Table 4.2 for the maximum cycling temperature for each sample. The sample number is 806.

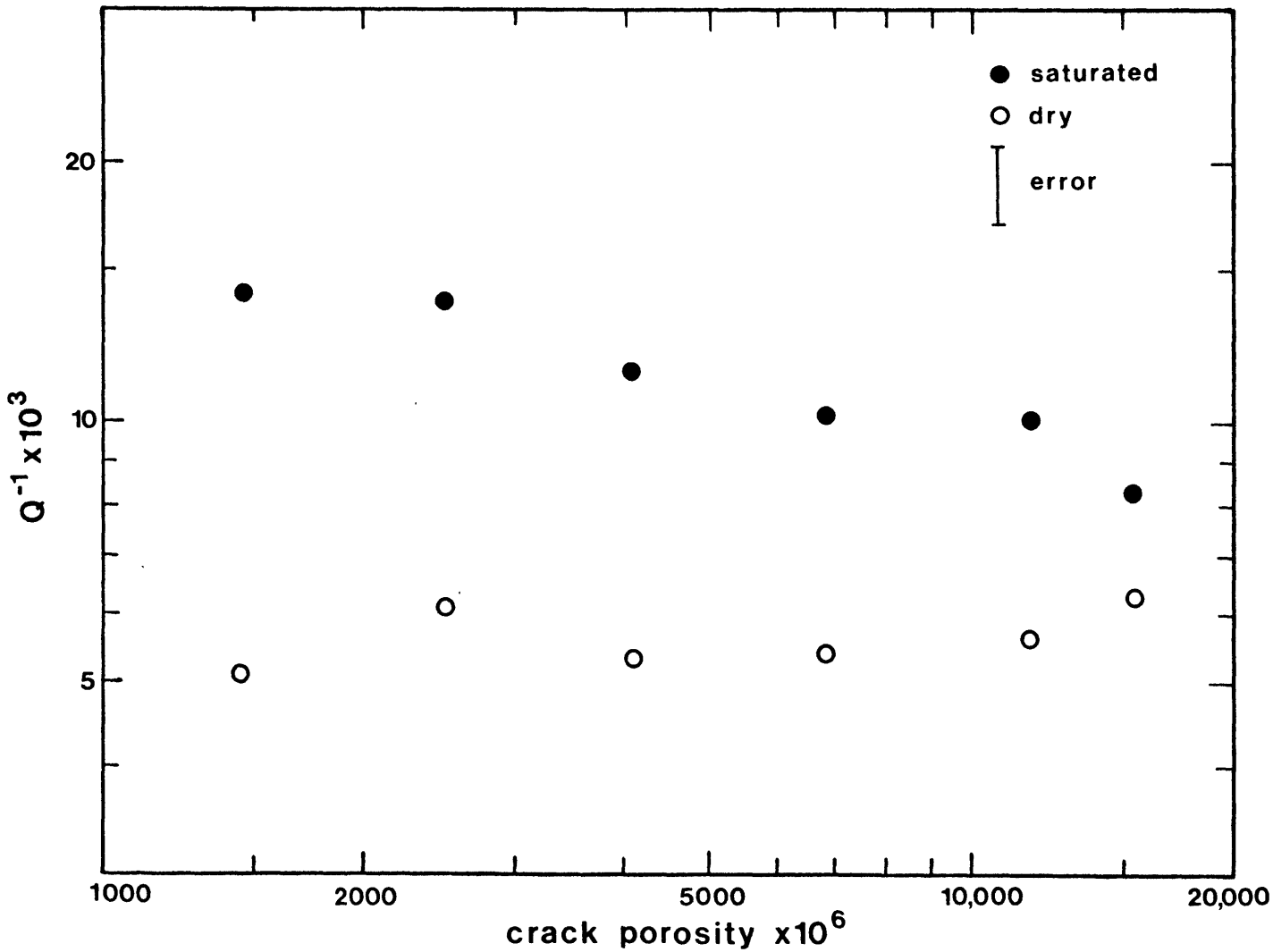
saturated
dry
error
20
10
5
$Q^{-1} \times 10^3$
1000
2000
5000
10,000
20,000
crack porosity $\times 10^6$

Table 4.3. Attenuation of thermally cycled Frederick diabase. Sample number is 1242. Crack porosities were not measured on these samples, but were calculated from the maximum cycling temperature according to the relation found by Simmons and Cooper (1978).

maximum cycling temperature, °C	crack porosity x 10^6 (±25%)	Q^{-1} x 10^3 dry	Q^{-1} x 10^3 saturated
25	<5	0.91	1.4
100	20	0.83	1.1
150	30	0.92	1.2
250	70	1.2	2.1
300	105		1.7
400	240	0.83	1.8
420	280	1.4	4.1
450	355	2.6	5.6
500	530	4.1	5.9

Fig. 4.3. Q^{-1} of thermally cycled Frederick diabase. Sample number is 1242. See Table 4.3 for the maximum cycling temperature for each sample.

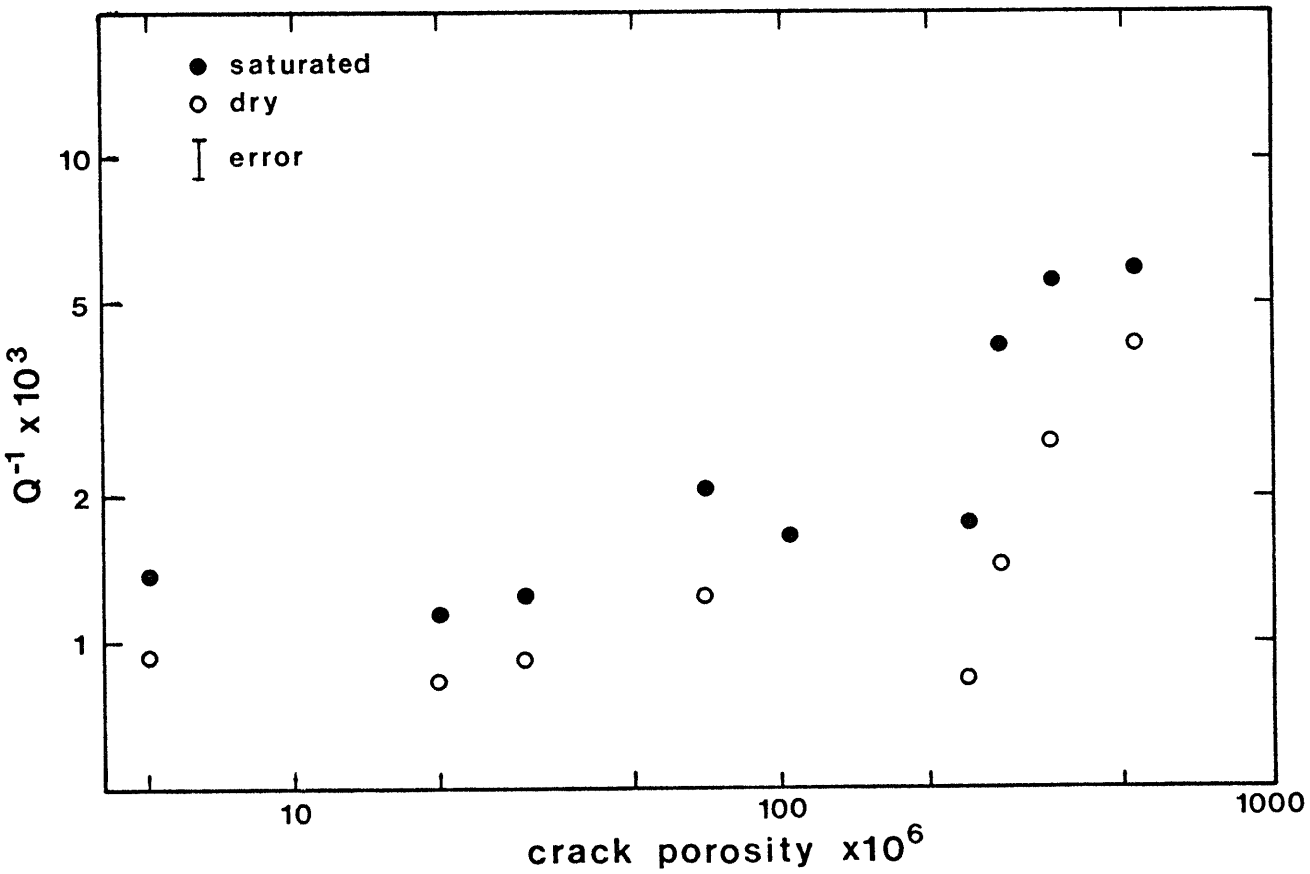
saturated
dry
error
10
5
2
1
$Q^{-1} \times 10^3$
10
100
1000
crack porosity $\times 10^6$

Table 4.4. Anisotropy of attenuation in Westerly granite and Chelmsford granite. See text for an explanation of ζ. ζ was determined from DSA measurements on a different sample cut from the same block of rock as the cores for the attenuation measurement. DSA data on sample 806 was collected and analyzed by M. L. Batzle.

direction	$Q^{-1} \times 10^3$ dry	$Q^{-1} \times 10^3$ saturated	ζ (80 bar) $\times 10^6$	ζ (2 kbar) $\times 10^6$
Westerly 806				
rift #1	5.6	19		
#2	5.6	17		
#3	6.0	18		
mean	5.7	18	18	590
grain #1	6.5	19		
#2	6.1	19		
#3	6.0			
mean	6.2	19	21	520
hardway #1	4.8	15		
#2	5.5	15		
#3	5.4	14		
#4	4.5	13		
mean	5.0	14	12	340
Chelmsford A757				
rift #1	7.3	19		
	7.7			
#2	9.8	20		
	9.4			
mean	8.6	19	27	1335
grain #1	9.5	18		
	10.4			
#2	7.4	18		
	6.7			
mean	8.5	18	15	475
hardway #1	6.6	22		
	7.8			
#2	6.6	21		
	8.1			
mean	7.3	22	6	560

note: rift, grain and hardway are defined in the Glossary, p 139.

at zero pressure that is attributable to the closure of cracks under hydrostatic confining pressure. Its variation with direction is a measure of the anisotropy of the crack distribution. The sum of ζ in three orthogonal directions is the standard crack porosity.

For Westerly granite, Q^{-1} is least in the hardway direction, which has the smallest value of ζ; and Q^{-1} is largest in the grain direction, which has intermediate ζ, although it has the largest ζ for cracks with closure pressures below 100 bars (i.e., low aspect ratio cracks). The anisotropy in Q^{-1} is less than the anisotropy in the crack distribution. The ratio of smallest to largest value of Q^{-1} is 0.81 in the dry case and 0.73 in the saturated case, while the ratio of smallest to largest ζ is 0.58.

The crack distribution of Chelmsford granite is more anisotropic than that of Westerly granite, but its Q^{-1} is nearly isotropic. In both dry and saturated cases there is no significant difference in Q^{-1} between the rift and grain directions, which have the largest and smallest values of ζ. The difference between Q^{-1} in the hardway direction and the values in the other two directions is only barely significant.

4.4 Effect of temperature on Q^{-1}

The variation of Q^{-1} as temperature was raised to between 500 and 600 °C for two cycles is shown in Fig. 4.4 for a diabase, #1401, and in Fig. 4.5 for Middlebrook felsite, #1407. Although sample 1401 has a higher Q^{-1} at

Fig. 4.4. Variation of Q^{-1} with temperature for sample 1401, a diabase. ●, first cycle ascending temperature; ▲, second cycle ascending temperature; ■, third cycle ascending temperature.

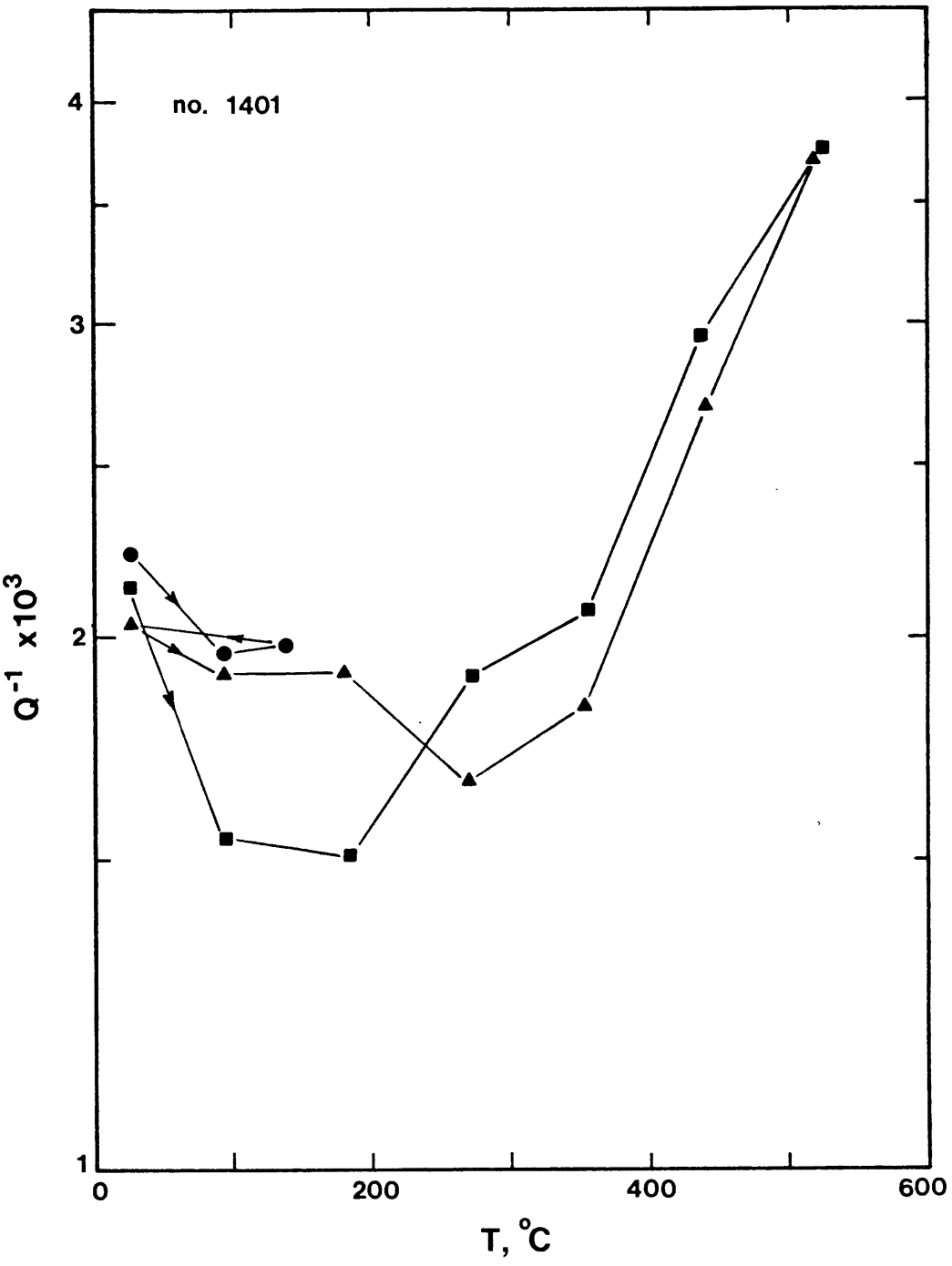
no. 1401
4
3
2
1
0
200
400
600
Q^{-1} x10^3
T, °C

Fig. 4.5. Variation of Q^{-1} with temperature for Middlebrook felsite, sample #1407. ●, first cycle ascending temperature; o, first cycle descending; ▲, second cycle ascending; ▵, second cycle descending.

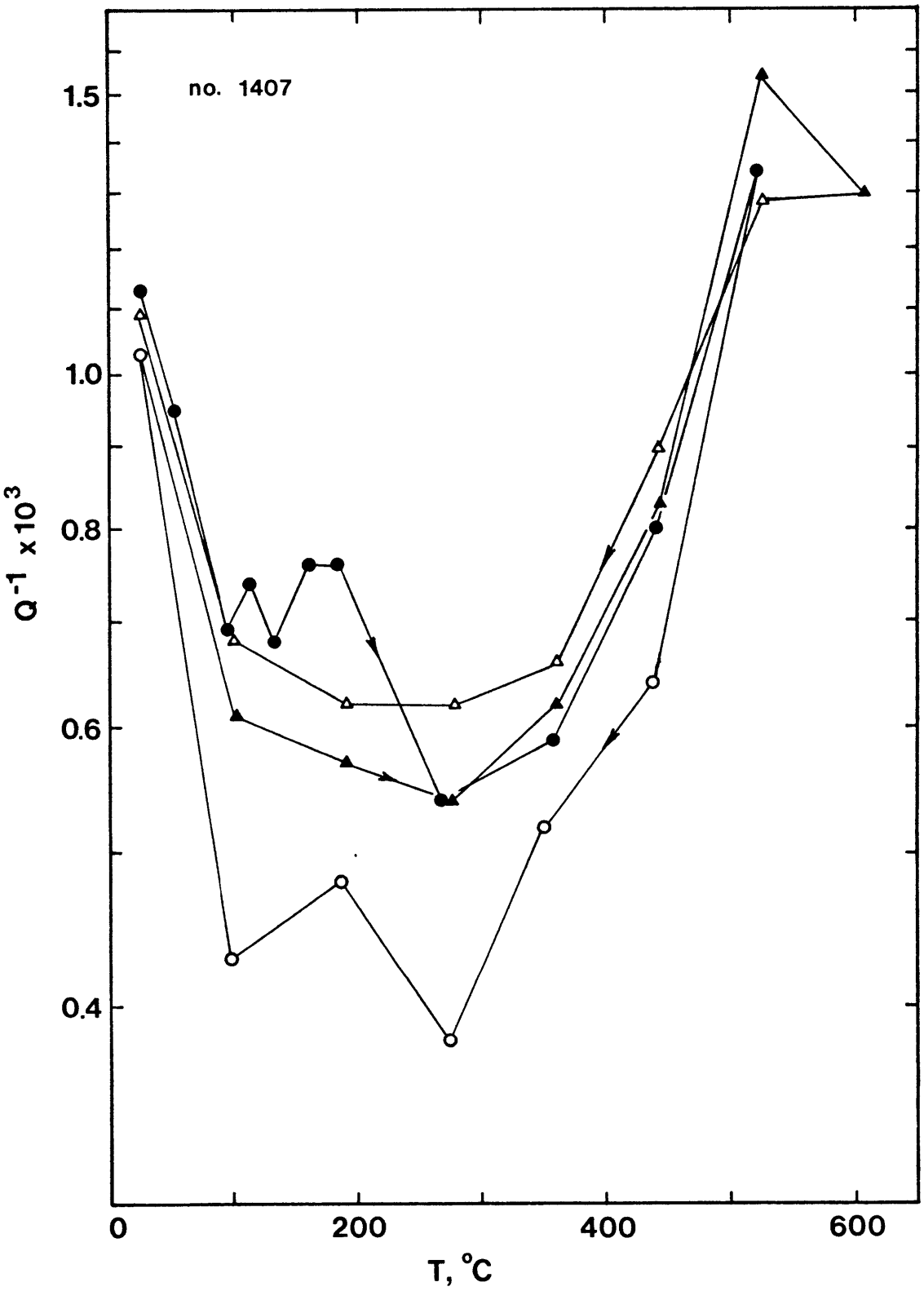
no. 1407
1.5
1.0
0.8
0.6
0.4
$Q^{-1} \times 10^3$
0
200
400
600
T, °C

all temperatures, both samples show the same general features. Q^{-1} initially decreases as temperature is raised, reaches a minimum between 200 and 300 °C, and then increases again at higher temperatures. There was little difference between the first and second heating cycles. The Q^{-1} at room temperature at the end of each cycle was equal to the initial value within the uncertainty of the measurement. The rate of increase in Q^{-1} between 300 and 500 °C was approximately the same for the two samples. For sample 1407, which has a greater initial crack porosity, the decrease in Q^{-1} between room temperature and 300 °C was more pronounced.

4.5 Effect of frequency on Q^{-1}

Attenuation was measured at several frequencies on four rocks: Westerly granite #1132 (collected at the same time as #1134), Wausau granite #1343, Graniteville granite #1409, and Skrainka diabase #1415. The results, shown in Fig. 4.6, show no significant frequency variation in Q^{-1} for dry rocks. The total frequency range is 0.14 to 2.5 Hz, although it was not possible to cover that entire frequency range with one sample. For saturated Westerly granite there was a significant difference in Q^{-1} between two samples measured at frequencies of 0.69 and 1.87 Hz.

4.6 Effect of amplitude on Q^{-1}

Figure 4.7 shows Q^{-1} measured over a range of strain amplitudes for three rocks when dry, Chelmsford granite

Fig. 4.6. Variation of Q^{-1} with frequency. Sample 1132 is Westerly granite, 1409 is Graniteville granite, 1343 is Wausau granite, 1415 is Skrainka diabase.

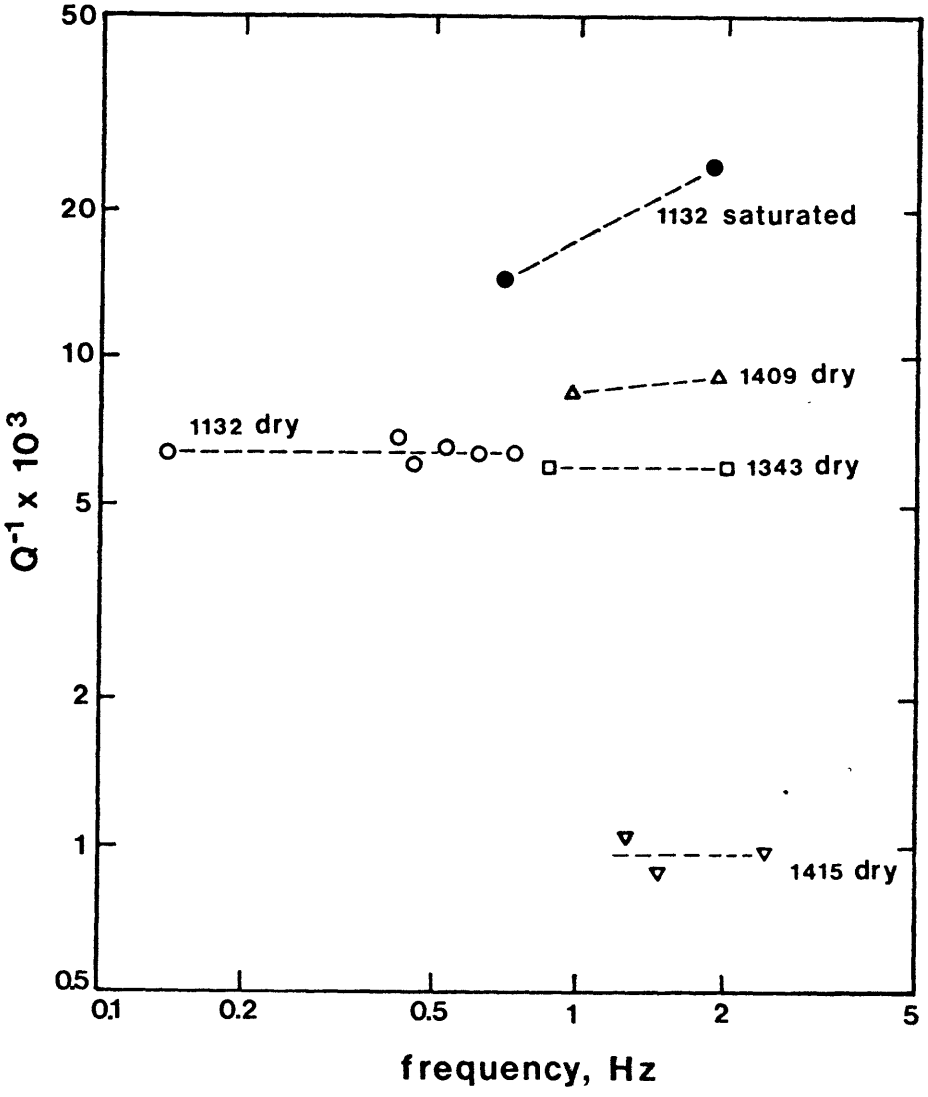
50
20
10
5
2
1
0.5
0.1
0.2
0.5
1
2
5
$Q^{-1} \times 10^3$
frequency, Hz
1132 saturated
1409 dry
1132 dry
1343 dry
1415 dry

Fig. 4.7. Variation of Q^{-1} with strain amplitude. Sample A757 is Chelmsford granite, 1328 is a gabbro from Hurley, Wi, 1242 is Frederick diabase.

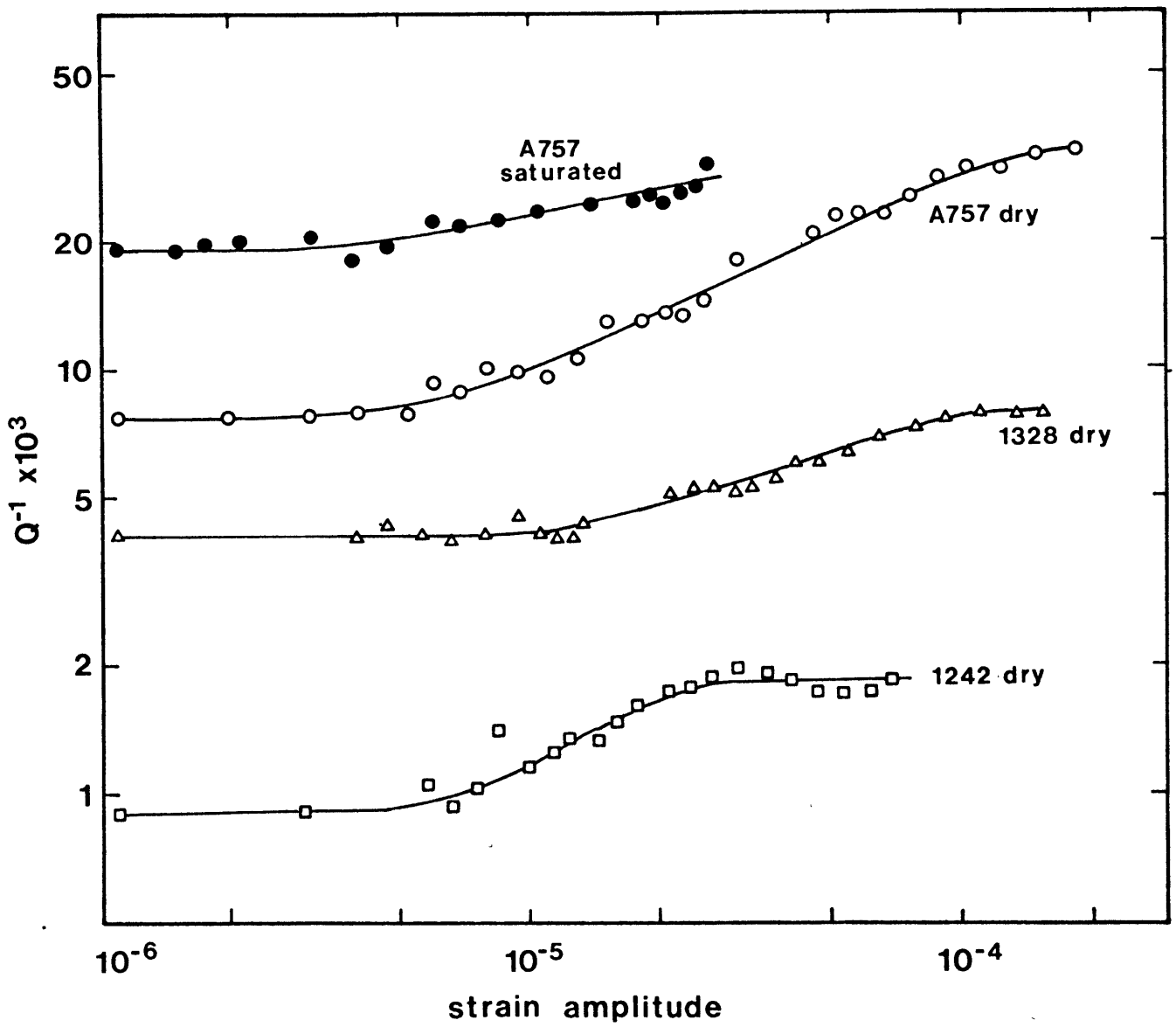
50
20
10
5
2
1
Q^{-1} x10^3
A757
saturated
A757 dry
1328 dry
1242 dry
10^{-6}
10^{-5}
10^{-4}
strain amplitude

#A757, Frederick diabase #1242, and Mellen gabbro #1328; and Chelmsford granite when saturated. All three samples have constant Q^{-1} at low strains, a range of increasing Q^{-1}, and constant Q^{-1} again at still higher strains. The strains at which the transitions between constant and increasing Q^{-1} occur differ among the samples. For samples 1242 and 1328, Q^{-1} increases by a factor of 2 between low and high strains, for A757 by a factor of 4 in the dry case. In saturated Chelmsford granite, amplitudes were not sufficiently high to see whether Q^{-1} became constant again, but the amount of increase over the range of strains observed is similar to the dry case.

Chapter 5

DISCUSSION

5.1 Dry rocks

The Q^{-1} of eighteen igneous rocks was found to be proportional to the square root of the crack porosity. Crack porosity is not likely to be the only determining factor, however, since most other physical properties that are affected by the presence of cracks depend not only on crack porosity but also on other geometrical properties of the cracks such as shape, width, or degree of connectivity. For example, theoretical analyses show that elastic properties depend on crack density ϵ, or equivalently, crack porosity divided by aspect ratio (Walsh 1965, Kuster and Toksoz 1974, Budiansky and O'Connell 1976). Instead, the fit to the square root of crack porosity is probably due to a similarity in the geometry of the cracks among the rocks. A relation does exist between the crack porosities of the rocks and the crack density parameter of O'Connell and Budiansky (1974) and Budiansky and O'Connell (1976).

The crack density ϵ is defined as

$$\epsilon = \frac{2}{\pi} N_V \left\langle \frac{A^2}{P} \right\rangle \tag{5.1}$$

where N_V is the number of cracks per unit volume, A is the

area and P is the perimeter of a crack, and the brackets denote average value. If the cracks are approximated as thin oblate spheroids of semi-major axis a and semi-minor axis c, $\epsilon = N_V \langle a^3 \rangle$. The volume of each spheroid is $v = (4\pi/3)a^2c = (4\pi/3)a^3\alpha$, where $\alpha = c/a$ is the aspect ratio of the crack. Therefore,

$$\epsilon = \frac{3}{4\pi} N_V \left\langle \frac{v}{\alpha} \right\rangle \tag{5.2}$$

In the simple case when all the cracks are the same size and aspect ratio,

$$\epsilon = \frac{3}{4\pi} \frac{\eta_c}{\alpha} \tag{5.3}$$

where η_c is the crack porosity. If a different shape is chosen to approximate the cracks, only the numerical constant changes, for example to $(1/2\pi)$ for discs or square plates.

The crack densities of the set of rocks were calculated from the compressibilities at 0 and 2 kbar using the equation for dry rocks given by Budiansky and O'Connell (1976):

$$\frac{\beta}{\bar{\beta}} = 1 - \frac{16\left(1 - \bar{\nu}^2\right)}{9\left(1 - 2\bar{\nu}\right)}\epsilon \tag{5.4}$$

where

$\bar{\nu}$ = effective Poisson's ratio and is the solution of the equation

$$\epsilon = \frac{45\ (\nu - \bar{\nu})(2 - \bar{\nu})}{16\ (1 - \bar{\nu}^2)(10\nu - 3\nu\bar{\nu} - \bar{\nu})} \tag{5.5}$$

$\bar{\beta}$ = effective compressibility, the measured value at zero kbar confining pressure

β = matrix compressibility, taken equal to the measured value at 2 kbar confining pressure

ν = matrix Poisson's ratio, taken equal to 0.2 for granites and felsites and 0.25 for diabases and gabbros. (Simmons and Brace (1965) measured ν = 0.21 for Westerly granite, 0.18 for Stone Mountain granite, and 0.25 for Frederick diabase at 10 kbar.) The crack densities were calculated by solving (5.4) and (5.5) iteratively given the measured compressibilities and the assumed matrix Poisson's ratio, and they are listed in Table 3.1.

Since crack porosity and crack aspect ratio ought to be independent, there is no reason to expect a systematic relation between ϵ and η_c among a set of rocks. For this set of rocks there is however, as shown in Fig. 5.1, perhaps reflecting a common origin for the cracks in these igneous rocks. The crack density is proportional to crack porosity to the 3/4 power. The least squares straight line fit between $\log(\epsilon)$ and $\log(\eta_c)$ is

$$\log(\epsilon) = 1.59 + 0.74 \log(\eta_c) \tag{5.6}$$

If the slope is set to exactly 3/4, the fit line becomes

$$\epsilon = 41 \eta_c^{3/4} \tag{5.7}$$

Since Q^{-1} is proportional to $\eta_c^{1/2}$ for this set of rocks, Q^{-1} is proportional to $\epsilon^{2/3}$. Substituting (5.7) into (4.4) and (4.6) we obtain for room dry rocks

$$Q^{-1} = 0.014 \epsilon^{2/3} \tag{5.8}$$

and for saturated rocks

Fig. 5.1. Variation of crack density with crack porosity. The data can be found in Table 3.1. Crack porosities were determined by differential strain analysis. Crack densities were calculated from compressibility by the method described in the text.

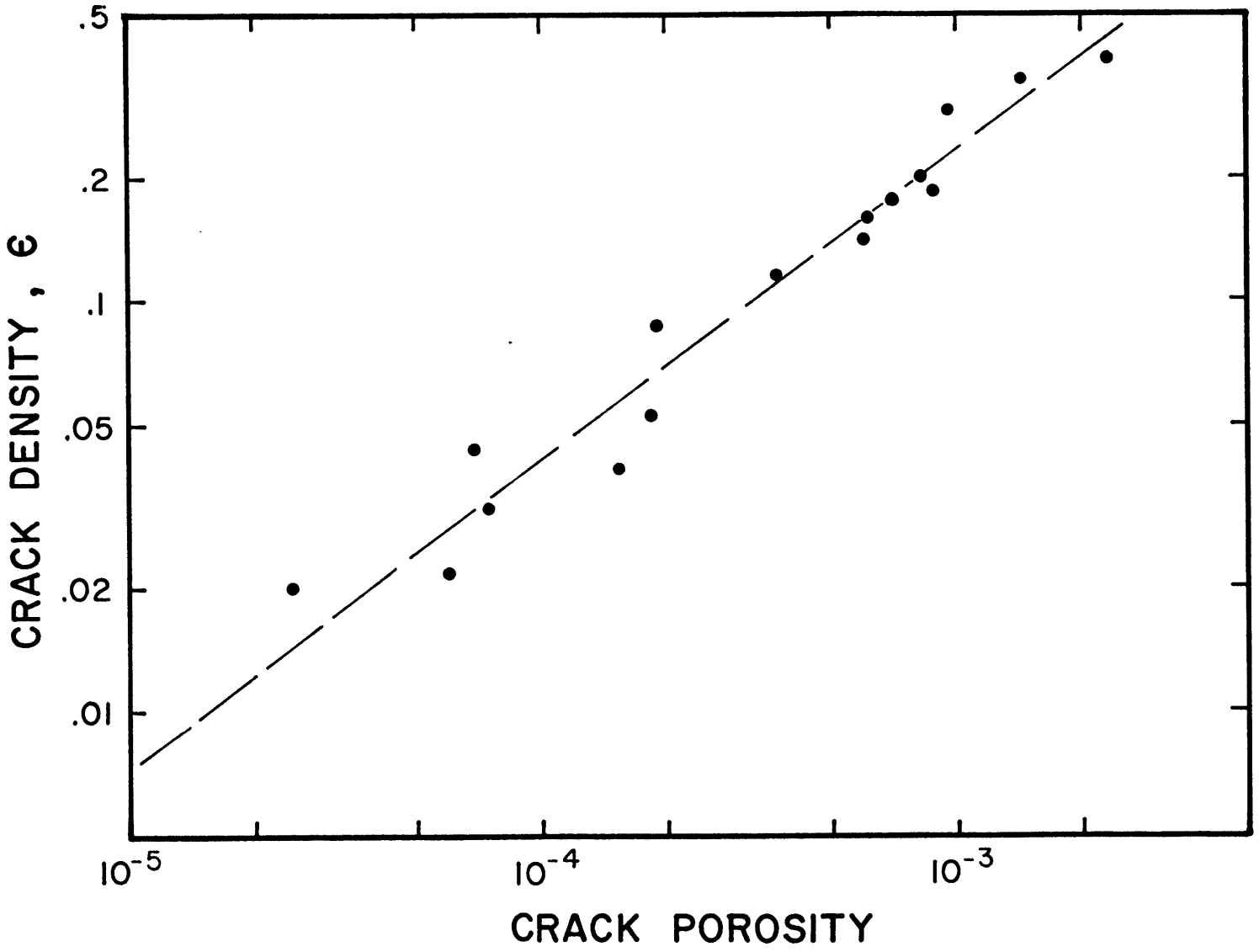
.5
.2
.1
.05
.02
.01
CRACK DENSITY, ϵ
10^{-5}
10^{-4}
10^{-3}
CRACK POROSITY

$$Q^{-1} = 0.033\ \epsilon^{2/3} \qquad (5.9)$$

The relations found between Q^{-1} and crack porosity and crack density do not help to distinguish among the attenuation models summarized in Sec. 1.4, since they predict different types of behaviour. Walsh's (1966) friction model predicts Q^{-1} to be proportional to ϵ, Mavko's (1979) friction model predicts Q^{-1} to be proportional to ϵ/α and to strain amplitude, and the fluid flow models of O'Connell and Budiansky (1977) and Mavko and Nur (1979) predict Q^{-1} to be proportional to $\omega\epsilon/\alpha^3$ in the low frequency regime, which probably includes 1 Hz.

The discrepancy between the models and the empirical relations derived from the data may be due to:

1. The reliance of the models on the elastic solution for either an isolated ellipsoid or an isolated two-dimensional crack of elliptical cross section to describe the strain at crack surfaces; or

2. The use of the total measured crack porosity or crack density, when in room dry rock only those cracks sufficiently narrow to contain adsorbed and capillary water contribute to attenuation and in saturated rock only those cracks with relaxation times for fluid flow near 1 second contribute to attenuation at 1 Hz.

5.2 Saturated rocks

The observation that Q^{-1} is about 2.3 times as large for the saturated samples as for the dry samples at 1 Hz

means that fluid flow is an important attenuation mechanism at that frequency. The variation of Q^{-1} with frequency in saturated rocks (Figs. 1.1 and 4.6) is also characteristic of fluid flow. The increase in frictional dissipation due to the wide cracks that become filled with fluid when the rock is saturated is insignificant because the friction coefficient for thick film lubrication is very low, 0.01 or less. The most likely mechanism between 1 and 10^5 Hz is fluid flow between cracks (O'Connell and Budiansky 1977). This mechanism can explain the observed attenuation with reasonable crack volumes and aspect ratios, as will be shown using differential strain analysis data for Westerly granite. To apply the analysis of O'Connell and Budiansky (1977) the distribution of crack density with aspect ratio is needed. This distribution can be calculated from the DSA data, with the usual assumption that the cracks are ellipsoids. DSA provides the volume of cracks ζ_v that are closed by the hydrostatic crack closure pressure P_c. P_c can be converted to aspect ratio using the results of Walsh (1965):

$$P_c = \left\{ \begin{array}{l} \dfrac{\pi E \alpha}{4(1-\nu^2)} = 4.6 \times 10^5 \, \alpha, \text{ penny shaped cracks} \\ \dfrac{E\alpha}{3(1-\nu^2)} = 1.95 \times 10^5 \, \alpha, \text{ plane strain} \\ \dfrac{E\alpha}{3} = 1.87 \times 10^5 \, \alpha, \text{ plane stress} \end{array} \right\} \quad (5.10)$$

where E is the Young's modulus of the matrix, ν is the Poisson's ratio of the matrix, and α is the crack aspect ratio. The values of E = 0.56 Mbar and ν = 0.21, measured

by Simmons and Brace (1965) for Westerly granite at 10 kbar were used. The crack density for each aspect ratio can be calculated from $\epsilon = (3/4\pi)\zeta_v/\alpha$. The results are given in Table 5.1. An average of the plane strain and plane stress assumptions was used to calculate the aspect ratios since the penny shaped assumption gives a total crack density of 0.88 by this calculation, much higher than the value of 0.35 calculated from the compressibilities (Table 3.1). The average of the plane strain and plane stress assumptions gives a total crack density of 0.269, somewhat low, but sufficiently close to demonstrate the general features of the fluid flow mechanism. The expression for Q^{-1} given by O'Connell and Budiansky (1977) is

$$Q^{-1} = \frac{32(1-\nu)}{45}\sum_i \frac{\omega\,\tau_{1i}\,\epsilon_i}{1+(\omega\tau_{1i})^2} + \frac{32(1-\nu)}{15(2-\nu)}\sum_i \frac{\omega\,\tau_{2i}\,\epsilon_i}{1+(\omega\tau_{2i})^2} \qquad (5.11)$$

where the non self-consistent formulas are used to simplify the calculations and

τ_{1i} = relaxation time for flow between cracks

$$= \frac{16(1-\nu)^2\, G\,\eta}{9(1-2\nu)\,\bar{G}\,K\,\alpha_i^3}$$

τ_{2i} = relaxation time for shear dissipation within cracks

$$= \frac{4(1-\nu)\,\eta}{\pi(2-\nu)\,\bar{G}\,\alpha_i}$$

G = matrix shear modulus

$\bar{G}$ = effective shear modulus of the cracked rock

Table 5.1. Crack density versus aspect ratio distribution of Westerly granite #806. See text for method of calculation.

closure pressure P_c, bar	$\zeta_v \times 10^6$	$\Delta\zeta_v \times 10^6$	aspect ratio α	crack density ϵ
0	0.0			
		0.03	4×10^{-6}	0.002
1.3	0.03			
		0.37	1.25×10^{-5}	0.006
4.3	0.4			
		1.3	4×10^{-5}	0.008
13	1.7			
		10	1.25×10^{-4}	0.019
43	11.7			
		184	4×10^{-4}	0.110
130	196			
		484	1.25×10^{-3}	0.092
430	680			
		430	4×10^{-3}	0.026
1300	1110			
		340	1.25×10^{-2}	0.006
2500	1450			

K = matrix bulk modulus

η = fluid viscosity

The results of substituting the values of crack density and aspect ratio from Table 5.1 into (5.11) for frequencies between 10^{-2} and 10^{8} Hz are shown in Fig. 5.2. Smooth curves were drawn through the calculated points which are scattered because of the discrete aspect ratio distribution. The bottom curve is the contribution to Q^{-1} of the loss due to the fluid flow. The top curve is the sum of the calculated fluid-flow Q^{-1} and the measured dry Westerly Q^{-1} of 5.7×10^{-3}; it is the predicted Q^{-1} for saturated Westerly granite. It has the type of variation with frequency shown in Fig. 1.1 for measurements by several investigators on different rocks. The peak in the middle of the figure is due to fluid flow between cracks. Shear relaxation in the fluid causes the rise in Q^{-1} at frequencies greater than 10^{6} Hz but is not important at lower frequencies. The predicted value of Q^{-1} at 0.7 Hz is approximately half the measured value but this discrepancy is not serious since the shape of the Q^{-1} curve is reasonable and the position of the peak must be regarded as being approximate. τ_1 depends on $1/\alpha^3$, so a factor of 2 change in estimated crack aspect ratio moves the peak by almost an order of magnitude in frequency. Also, the expression used for τ_1 is an estimate and other expressions are possible, each of which would place the peak at a different frequency. The important point of Fig. 5.2 is that the mechanism of fluid flow

Fig. 5.2. Predicted variation of Q^{-1} of saturated Westerly granite with frequency. See text for method of calculation. Bottom curve is Q^{-1} due to fluid flow. Top curve is th sum of the fluid flow and friction contributions to Q^{-1}. It is the predicted Q^{-1} for saturated Westerly granite.

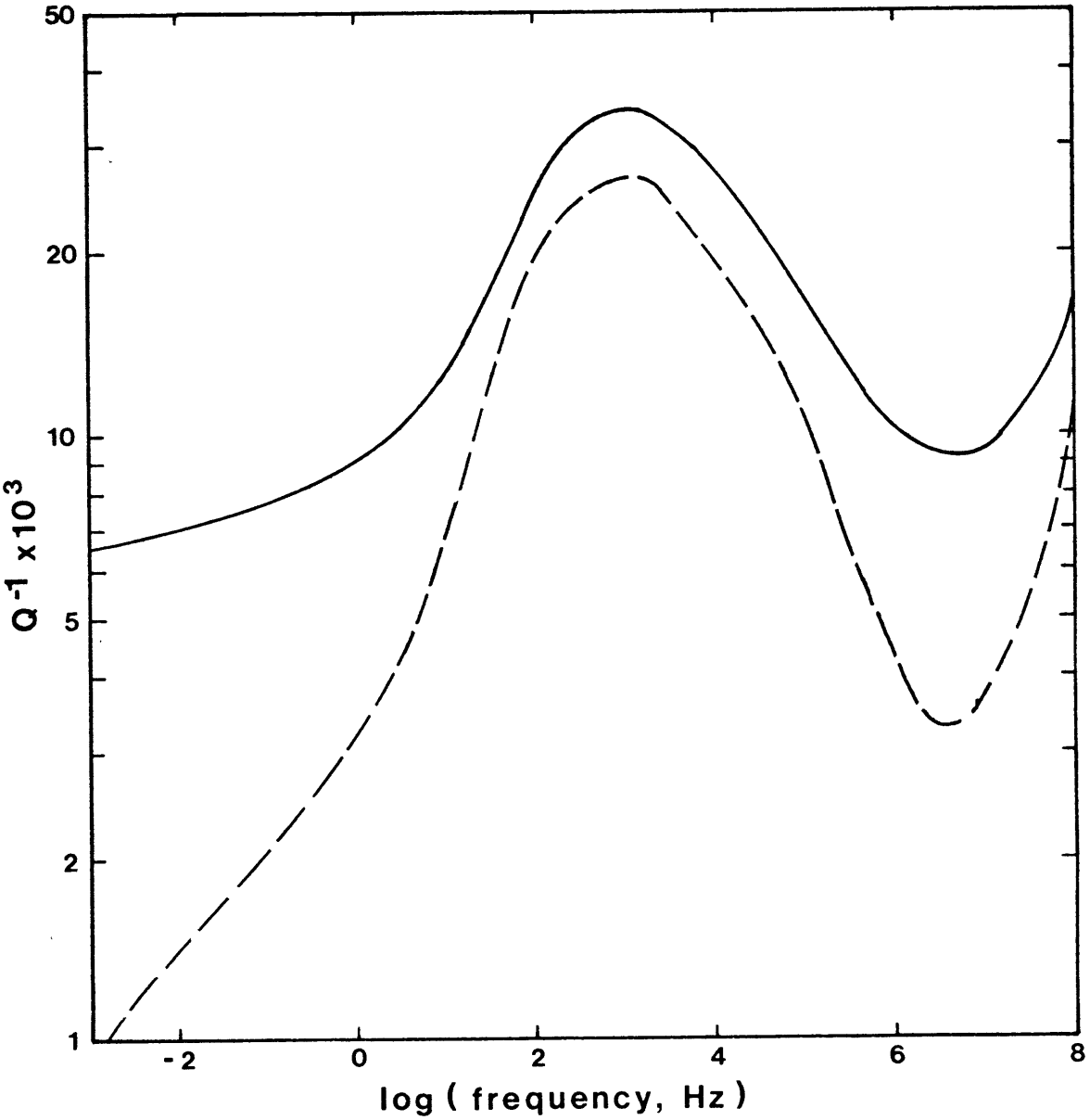
50
20
10
5
2
1
$Q^{-1} \times 10^3$
-2
0
2
4
6
8
log (frequency, Hz)

between cracks, or squirt flow, predicts a value of Q^{-1} near the observed value and a frequency dependence that is approximately what is observed.

5.3 Thermally cycled rocks

The sets of attenuation data of the thermally cycled Westerly granite and Frederick diabase, Figs. 4.2 and 4.3, differ from each other and from the results of normal igneous rocks. The differences can be related to changes in crack geometry with thermal cycling. Thermal cycling (i) produces new cracks, predominately at grain boundaries, where stresses due to the differential thermal expansion between grains are greatest; and (ii) widens existing cracks (Sprunt and Brace 1974). The new cracks, although irregular in shape, have parallel sides (Batzle et al 1979).

In dry thermally cycled rocks there is little change in Q^{-1} from the initial state. Therefore, either the new cracks are sufficiently wide, greater than about 200 Å in width, that they do not contribute to frictional dissipation, or the thermal cycling widens the existing cracks in the rock, removing enough of them from the portion contributing to friction to compensate for any new thin cracks produced.

For saturated Frederick diabase samples, Q^{-1} increases as crack porosity increases, as would be expected. Since the uncycled rock has essentially no cracks (as far as we can determine from differential strain analysis), thermal cycling produces new cracks that contribute to fluid flow

attenuation. For saturated Westerly granite samples, Q^{-1} decreases as crack porostiy increases. A possible explanation for this decrease is the following. Much of the increased porosity is due to the widening of pre-existing cracks (Batzle et al 1979). Also, the many new cracks formed must intersect other cracks, decreasing their effective lengths. The effect of this crack widening and shortening is to increase the effective aspect ratio of the cracks, that is, to decrease the relaxation time τ_1, which moves the attenuation due to fluid flow to higher frequencies. As the crack porosity of the samples increases, 1 Hz falls more and more on the low frequency side of the Q^{-1} peak shown in Fig. 5.2.

5.4 Effect of temperature

As mentioned in Chap. 2, the decrease in Q^{-1} as T is raised to 300 °C is explained by evaporation of the boundary lubricant film of adsorbed water, reducing the crack area involved in frictional dissipation. The increase in Q^{-1} at higher temperatures is a thermally activated mechanism, perhaps grain boundary relaxation (Jackson 1969, Jackson and Anderson 1970). In polycrystalline alumina and forsterite the grain boundary relaxation peak occurs at half the melting temperature at a frequency of 1 Hz (Jackson 1969). Half the melting temperatures of the constituent minerals of samples 1401 and 1407 range from 415 °C for albite to 670 °C for quartz. For sample 1407, a peak in Q^{-1} was found

between 500 and 600 °C, in the expected range. For sample 1401, a temperature sufficient to determine the presence of a peak was not reached. This interpretation of the increase in Q^{-1} as grain boundary relaxation is tentative, since the peak is defined by only one point. Other thermally activated creep mechanisms may contribute to attenuation at high temperatures. Further measurements to determine the effects of grain size, higher temperatures, and frequency are needed before the mechanism can be identified.

5.5 Anisotropy of attenuation

The torsional oscillation used in this study averages in an azimuthal sense the effect of cracks of different orientations, so that the observed anisotropy in Q^{-1} is less than it would be for plane polarized shear waves. This averaging partly explains why the anisotropy observed in Q^{-1} is less than the anisotropy in ζ. However, there must be additional factors not evident from DSA, since Q^{-1} is less anisotropic in Chelmsford granite than in Westerly granite, while ζ is more anisotropic in Chelmsford. In fact, in the dry Chelmsford cores, considering the range in Q^{-1} in a single direction, there is no significant anisotropy in Q^{-1}. The lack of anisotropy in Q^{-1} in dry Chelmsford granite could be explained if we assume that the narrow cracks contributing to frictional dissipation, unlike the total crack distribution, are uniformly oriented, but we have no means of testing that assumption at present. For the

saturated Chelmsford cores, the two cores in each direction agree very well, but the difference between the largest and smallest values of Q^{-1} is only 20%. The largest value of Q^{-1} is not found in the rift direction, as expected from the ζ values. Perhaps the details of connectivity of cracks of different orientations influences saturated Q^{-1} in this rock.

In Chelmsford granite the rift, grain, and hardway directions are not the axes of symmetry of the crack distribution (Simmons et al 1975), but in Westerly granite they are approximately (Siegfried and Simmons 1978). Assuming that the crack distribution in Westerly has orthorhombic symmetry, as it does in Chelmsford (Simmons et al 1975), the complex modulus formulation of Q^{-1} can be used to decompose the torsional Q^{-1}'s into the Q^{-1}'s corresponding to the single shear moduli c_{44}, c_{55}, and c_{66}.

For a rock with orthorhombic symmetry, torsion along the symmetry axes x_i is described by apparent shear moduli G_i that are simple combinations of the compliances s_{44}, s_{55}, and s_{66} (see Appendix A):

$$\left.\begin{aligned} G_1 &= \frac{2}{(s_{55}+s_{66})} \\ G_2 &= \frac{2}{(s_{44}+s_{66})} \\ G_3 &= \frac{2}{(s_{44}+s_{55})} \end{aligned}\right\} \quad (5.12)$$

The modulus G_1 can be written as (Nowick and Berry 1972, O'Connell and Budiansky 1978):

$$G_1 = G_1^R + iG_1^I \tag{5.13}$$

where G_1^R is the shear modulus of the core with its axis in the x_1 direction, $i = \sqrt{-1}$, and G_1^I is given by $Q_1^{-1} = G_1^I/G_1^R$, where Q_1^{-1} is the Q^{-1} of the core with its axis in the x_1 direction; and similarly for G_2 and G_3. The compliances are written as $s_{44} = s_{44}^R - is_{44}^I$ and similarly for s_{55} and s_{66}. Substituting the complex compliances into (5.12) gives

$$\begin{aligned} G_1 &= \frac{2}{(s_{55}^R+s_{66}^R) - i(s_{55}^I+s_{66}^I)} \\ &= \frac{2(s_{55}^R+s_{66}^R) + 2i(s_{55}^I+s_{66}^I)}{(s_{55}^R+s_{66}^R)^2 + (s_{55}^I+s_{66}^I)^2} \end{aligned} \tag{5.14}$$

Therefore,

$$Q_1^{-1} = \frac{G_1^I}{G_1^R} = \frac{s_{55}^I + s_{66}^I}{s_{55}^R + s_{66}^R} \tag{5.15}$$

and similarly,

$$Q_2^{-1} = \frac{G_2^I}{G_2^R} = \frac{s_{44}^I + s_{66}^I}{s_{44}^R + s_{66}^R} \tag{5.16}$$

$$Q_3^{-1} = \frac{G_3^I}{G_3^R} = \frac{s_{44}^I + s_{55}^I}{s_{44}^R + s_{55}^R} \tag{5.17}$$

The data for dry Westerly granite, with the rift, grain, and hardway directions as the x_1, x_2, and x_3 axes respectively, are:

$$\left.\begin{aligned} Q_1^{-1} &= 5.72 \times 10^{-3} \\ Q_2^{-1} &= 6.20 \times 10^{-3} \\ Q_3^{-1} &= 5.05 \times 10^{-3} \end{aligned}\right\} \quad (5.18)$$

The cores were 0.28 cm in radius and 5.8 cm long and the frequencies of oscillation were $f_1 = 0.663$ Hz, $f_2 = 0.649$ Hz and $f_3 = 0.685$ Hz. Substituting these numbers in a rearranged form of (3.4),

$$G = \frac{8\pi f^2 LJ}{a^4}, \quad (5.19)$$

the torsional moduli are $G_1 = 0.17$ Mb, $G_2 = 0.16$ Mb, and $G_3 = 0.18$ Mb. Using these moduli and (5.18) in (5.15) to (5.17), the compliances and the corresponding Q^{-1}'s are:

$$\left.\begin{aligned} s_{44} &= 5.8 \text{ Mb}^{-1}, \; Q_{44}^{-1} = 5.6 \times 10^{-3} \\ s_{55} &= 5.3 \text{ Mb}^{-1}, \; Q_{55}^{-1} = 4.5 \times 10^{-3} \\ s_{66} &= 6.6 \text{ Mb}^{-1}, \; Q_{66}^{-1} = 6.7 \times 10^{-3} \end{aligned}\right\} \quad (5.20)$$

Since for an orthorhombic solid $c_{44} = 1/s_{44}$, $c_{55} = 1/s_{55}$, and $c_{66} = 1/s_{66}$, the shear moduli are $c_{44} = 0.17$ Mb, $c_{55} = 0.19$ Mb, and $c_{66} = 0.15$ Mb. The modulus c_{44} relates the shear stress τ_{23} to the shear strain ε_{23}, c_{55} relates the stress τ_{13} to the strain ε_{13}, and c_{66} relates the stress τ_{12} to the strain ε_{12}. If friction on crack surfaces is the cause of attenuation, and if we assume that the distribution of narrow cracks that contribute to friction is similar to the distribution of ζ, Q_{66}^{-1} should be the largest, as is observed, since ζ_1 and ζ_2 are larger than ζ_3, i.e. there are more cracks normal to the x_1 and x_2 directions than normal

to the x_3 direction. Since ζ_1 is larger than ζ_2, Q_{55}^{-1} should be larger than Q_{44}^{-1}, opposite to what is observed. However, ζ_2 is larger than ζ_1 at pressures less than 100 bars, which means that there are more low closure pressure or low aspect ratio cracks normal to the x_2 direction, and perhaps also more narrow cracks.

For the saturated Westerly cores a similar calculation results in:

$$\left.\begin{aligned} c_{44} &= 0.14 \text{ Mb}, \; s_{44} = 7.0 \text{ Mb}^{-1}, \; Q_{44}^{-1} = 1.5 \times 10^{-2} \\ c_{55} &= 0.16 \text{ Mb}, \; s_{55} = 6.1 \text{ Mb}^{-1}, \; Q_{55}^{-1} = 1.3 \times 10^{-2} \\ c_{66} &= 0.13 \text{ Mb}, \; s_{66} = 7.8 \text{ Mb}^{-1}, \; Q_{66}^{-1} = 2.3 \times 10^{-2} \end{aligned}\right\} \quad (5.21)$$

In saturated rocks, normal motions between crack faces cause much greater dissipation due to fluid flow than do shear motions (Mavko and Nur 1979). The relative magnitudes of the Q^{-1} values then should depend on the cracks at near 45° to the core axes, since the normal stress on cracks is greatest at that orientation in a torsional oscillation. Since ζ_1 and ζ_2 are similar and larger than ζ_3, there is a similar number of cracks oriented at 45° to the x_1 and x_3 axes and at 45° to the x_2 and x_3 axes, and a larger number oriented at 45° to the x_1 and x_2 axes. Therefore, Q_{66}^{-1} should be larger than Q_{44}^{-1} and Q_{55}^{-1}, which should be similar, as is observed.

5.6 Implications for the earth

The attenuations measured in this study were caused by the cracks in laboratory samples of rocks. The results

thus apply only to the upper few kilometers of the earth's crust where cracks exist. The occurrence of cracks in crustal rocks in situ is not well known. Below the weathered zone, cracks tend to heal or be sealed by minerals precipitated from pore fluids. The abundant healed and sealed cracks in igneous rocks (Richter and Simmons 1977), many of which are cross-cutting and thus of different ages, suggest that healing and sealing of cracks in the earth takes place relatively rapidly. In that case, cracks should occur in abundance only where they are continually being created, in active tectonic areas or near fault zones. In stable cratonic regions, microcracks should be absent or be of relatively low density at depths below one or two kilometers, except near fault zones. For example, Simmons and Nur (1968) noted that sonic and electrical logs from a 3.8 km deep borehole in Oklahoma and granitic sections of a 3.0 km deep borehole in Wyoming varied much less with depth than would be expected from laboratory measurements on granites containing microcracks, and they concluded that the rock in situ does not contain many microcracks, or that the microcracks are completely saturated with water. Wang and Simmons (1978) concluded that gabbroic rock at the bottom of a 5.3 km deep borehole in the Michigan Basin does not contain any microcracks in situ, based on microscopic observations and physical property measurements on core samples. Although the recovered core does contain microcracks, they interpret them to be due to stress relief. In other regions, open

microcracks may exist at depth. Simmons and Cooper (1976) concluded from differential strain analysis on core from the GT2 drillhole in New Mexico that although a large fraction of the observed microcrack porosity in the core samples was produced during drilling and retrieval of the core, the core samples do contain microcracks that would be open in situ. They estimated that the in situ crack porosity at 2.9 km depth is 100×10^{-6}, a value that may be representative of crustal rocks in the vicinity of active geothermal systems, but is unlikely to be typical of the crust outside active tectonic areas. Besides intergranular microcracks, larger scale discontinuities such as joints, fracture zones, and faults occur in the crust. Their importance to the average attenuation of the crust depends on their volume or surface area compared to that of the microcracks when averaged over representative rock volumes.

Some shear wave Q^{-1} models of different regions of the crust determined from inversion of surface wave attenuation data (Mitchell 1975, Canas and Mitchell 1978) and from simultaneous inversion of surface wave attenuation and phase velocity (Lee and Solomon 1979) are given in Table 5.2, along with the crack porosities required to produce the Q^{-1} values, according to Eq. 4.6. For North America, Mitchell (1975) found that Q^{-1} averages 4×10^{-3} in the upper 15 km in eastern North America and 8×10^{-3} in the upper 15 km of western North America. In both regions Q^{-1} decreases to 1×10^{-3} at depths between 20 and 40 km. In the upper 15 km,

Table 5.2. Regional variation of Q^{-1} of the crust and interpretation as regional variation in crack porosity. Crack porosity (η_c) was calculated from Q^{-1} by Eq. 4.6. Except where stated, Q^{-1} was assumed to be independent of frequency. For frequency dependent Q^{-1} models, the value at 1 Hz is given.

region	depth, km	$Q^{-1} \times 10^3$	$\eta_c \times 10^6$
Mitchell (1975):			
eastern North America	0 - 15	4	105
	20 - 40	1	5
western North America	0 - 15	8	420
	20 - 40	1	5
Lee and Solomon (1979):			
east-central North America	0 - 38	1.7 - 2.6	20 - 40
western North America	2 - 21	2.7 - 4.9	40 - 160
	21 - 45	0.6 - 2.5	2 - 40
$Q^{-1} \propto f^{-0.2}$:			
western North America	2 - 21	1.5 - 2.8	15 - 40
	21 - 45	0 - 1.5	0 - 15
$Q^{-1} \propto f^{-0.5}$:			
east-central North America	0 - 38	0.4 - 0.6	1 - 2
western North America	2 - 21	0.5 - 1.2	2 - 10
	21 - 45	0 - 1.1	0 - 10

Table 5.2 continued

region	depth, km	$Q^{-1} \times 10^3$	$\eta_c \times 10^6$
Lee and Solomon (1979):			
central Pacific	12 - 57	4.1 - 4.4	
Canas and Mitchell (1978):			
eastern Pacific	5 - 10	5 - 8	165 - 420
(less than 50 My old)	10 - 35	4 - 8	
	35 - 60	4	
central Pacific	5 - 10	4 - 7	105 - 320
(between 50 and 100 My old)	10 - 35	4 - 7	
	35 - 60	4	
western Pacific	5 - 10	2.5 - 4	40 - 105
(greater than 100 My old)	10 - 35	4 - 6	
	35 - 60	0.5 - 2	

the attenuation is due to cracks. The difference in Q^{-1} between the western and eastern regions may be due either to differences in crack porosity or saturation. If we assume that (i) the cracks are saturated and (ii) the geometry of the in situ cracks is similar to the geometry of the cracks in the rocks measured in this study, then from (4.6) the average crack porosity in the upper 15 km of the crust is 105×10^{-6} in eastern North America and 420×10^{-6} in western North America. The Q^{-1} of 1×10^{-3} between 20 and 40 km depth is approximately equal to the Q^{-1} measured on Frederick and Skrainka diabases, rocks containing very few microcracks. Lee and Solomon (1979) obtained lower estimates of Q^{-1}: between 1.7 and 2.6×10^{-3} for depths between 0 and 38 km in eastern North America; and between 2.7 and 4.9×10^{-3} for depths between 2 and 21 km in western North America. Average crack porosities in the upper crust of between 20 and 45×10^{-6} in the eastern region and between 50 and 160×10^{-6} in the western region would produce these Q^{-1} values. If Q^{-1} was allowed to be frequency dependent, the inversion produces lower Q^{-1}'s at 1 Hz, as shown in Table 5.2. If regions of the crust are not saturated, then the crack porosity required to produce the same value of Q^{-1} as the saturated case may be higher. Differences in saturation could also explain the difference in Q^{-1} between eastern and western North America; differences in crack porosity are not required.

Canas and Mitchell (1978) showed that Q^{-1} of the

lithosphere under the Pacific Ocean decreases as the age of the seafloor increases. For the shallowest layer, 5 to 10 km deep, the decrease in Q^{-1} can be attributed to the healing and sealing of cracks with time. At greater depths, the decrease in Q^{-1} can be attributed to cooling of the lithosphere with age.

The values of crack porosity given above should be regarded as being very approximate, since there is no reason to expect the geometry of in situ cracks in the crust to be the same as that in rocks collected at the surface of the earth. In situ crack porosities predicted from (4.6) are probably overestimates since lithostatic confining pressure will tend, we believe, to cause in situ cracks to be narrower in general than cracks in laboratory samples. If so, a greater fraction of in situ cracks will be sufficiently narrow to contribute to frictional dissipation, and Q^{-1} will be higher, than in a laboratory sample with the same total crack porosity.

Chapter 6

CONCLUSION

The main features of the attenuation data measured for this thesis are:

1. For a set of igneous rocks that range in crack porosity from <5 to 2370 x 10^{-6}, Q^{-1} at frequencies near 1 Hz is proportional to the square root of crack porosity, or the two-thirds power of crack density, in both dry and saturated rocks.

2. Q^{-1} for the rocks when saturated was 2.3 times Q^{-1} for the rocks when dry.

The main conclusions drawn from the data are:

1. Friction of crack surfaces lubricated by adsorbed water films can adequately explain the observed Q^{-1} of room dry rocks, its frequency independence, and the effects of temperature, pressure, and strain amplitude.

2. The flow of water between cracks can adequately explain the observed Q^{-1} of saturated rocks, and its frequency dependence.

3. An increase in Q^{-1} at temperatures above 300 or 400 °C is probably due to a thermally activated mechanism.

4. A reasonably small average crack porosity can explain the Q^{-1} of the crust determined from seismic surface wave attenuation measurements.

REFERENCES

Bailey, A. I., and J. S. Courtney-Pratt: The area of real contact and the shear strength of monomolecular layers of a boundary lubricant. Proc. Roy. Soc. A227, 500-515 (1955)

Batzle, M. L., G. Simmons, and R. W. Siegfried: Direct observation of fracture closure in rocks under stress. (abstract) EOS Trans. Am. Geophys. Union 60, 380 (1979)

Born, W. T.: The attenuation constant of earth materials. Geophysics 6, 132-148 (1941)

Bowden, F. P., and D. Tabor: The Friction and Lubrication of Solids (Pt. I). Clarendon Press (1964)

Bradley, J. J., and A. N. Fort Jr.: Internal friction in rocks. in: Handbook of Physical Constants, S. P. Clark, ed. Geol. Soc. Am. Memoir 97, 175-193 (1966)

Brennan, B. J., and F. D. Stacey: Frequency dependence of elasticity of rock -- test of seismic velocity dispersion. Nature 268, 220-222 (1977)

Bruckshaw, J. McG., and P. C. Mahanta: The variation of the elastic constants of rocks with frequency. Petroleum 17, 14-18 (1954)

Budiansky, B., and R. J. O'Connell: Elastic moduli of a cracked solid. Int. J. Solids & Structures 12, 81-97 (1976)

Canas, J. A., and B. J. Mitchell: Lateral variation of surface-wave anelastic attenuation across the Pacific. Bull. Seism. Soc. Am. 68, 1637-1650 (1978)

Cooper, H. W., and G. Simmons: The effect of cracks on the thermal expansion of rocks. Earth & Planetary Science Letters 36, 404-412 (1977)

Dale, T. N.: The commercial granites of New England. U. S. Geol. Survey Bull. 738 (1923)

Fairbairn, H. W., W. Schlecht, R. E. Stevens, W. Dennen, L. Ahrens, and F. Chayes: A cooperative investigation of precision and accuracy in chemical, spectrochemical, and modal analysis of silicate rocks. U. S. Geol. Survey Bull. 980 (1951)

Feves, M., G. Simmons, and R. W. Siegfried: Microcracks in crustal igneous rocks: physical properties. in: The Earth's Crust, Its Nature and Physical Properties. Geophysical Monograph 20, Am. Geophys. Union, 95-117 (1977)

Fisher, L. K., and J. N. Israelachvili: Direct experimental verification of the Kelvin equation for capillary condensation. Nature 277, 548-549 (1979)

Frazer, J. H.: An optical study of adsorbed films. Phys. Rev. 33, 97-104 (1929)

Frisillo, A. L., and T. J. Stewart: Effect of partial gas/brine saturation on ultrasonic absorption is sandstone. paper presented at Conference on Seismic Wave Attenuation, Stanford University, June 25-27, 1979, abstract in Stanford University Publications, Geological Sciences XVII, 24 (1979)

Gardner, G. H. F., M. R. J. Wyllie, and D. M. Droschak: Effects of pressure and fluid saturation of the attenuation of elastic waves in sands. J. Petroleum Tech. 16, 189-198 (1964)

Gordon, R. B.: Mechanical relaxation spectrum of crystalline rock containing water. J. Geophys. Res. 79, 2129-2131 (1974)

Gordon, R. B., and L. A. Davis: Velocity and attenuation of seismic waves in imperfectly elastic rock. J. Geophys. Res. 73, 3917-3935 (1968)

Gowd, T. N.: Changes in absorption of ultrasonic energy travelling through rock specimens stressed to fracture. Phys. Earth & Planetary Interiors 4, 43-48 (1970)

Hadley, K.: Comparison of calculated and observed crack densities and seismic velocities in Westerly granite. J. Geophys. Res. 81, 3484-3494 (1976)

Hagymassy, J., S. Brunauer, R. Sh. Mikhail: Pore structure analysis by water vapor adsorption. 1. t-curves for water vapor. J. Colloid & Interface Science 29, 485-491 (1969)

Hall, A. C.: Optical studies of thin films on surfaces of fused quartz. J. Phys. Chem. 74, 2742-2746 (1970)

Hamilton, E. L.: Compressional wave attenuation in marine sediments. Geophysics 37, 620-646 (1972)

Hearmon, R. F. S.: An Introduction to Applied Anisotropic Elasticity. Oxford (1961)

Heymann, F., E. Rabinowicz, and B. G. Rightmire: Friction apparatus for very low-speed sliding studies. Rev. Sci. Instr. 26, 56-58 (1955)

Holland, L.: The Properties of Glass Surfaces. Chapman and Hall (1964)

Jackson, D. D.: Grain Boundary Relaxations and the Attenuation of Seismic Waves. Ph.D. thesis, Massachusetts Institute of Technology (1969)

Jackson, D. D., and D. L. Anderson: Physical mechanisms of seismic wave attenuation. Rev. Geophys. & Space Physics 8, 1-63 (1970)

Johnson, K. L.: Surface interaction between elastically loaded bodies under tangential forces. Proc. Roy. Soc. A 230, 531-548 (1955)

Johnston, D. H.: The Attenuation of Seismic Waves in Dry and Saturated Rocks. Ph.D. thesis, Massachusetts Institute of Technology (1978)

Johnston, D. H., M. N. Toksoz, and A. Timur: Attenuation of seismic waves in dry and saturated rocks: II Mechanisms. Geophysics 44, 691-711 (1979)

Kissel, F. N.: Effect of temperature variation on internal friction in rocks. J. Geophys. Res. 77, 1420-1423 (1972)

Knopoff, L.: Q. Reviews of Geophysics 2, 625-660 (1964)

Knopoff, L., and L. D. Porter: Attenuation of surface waves in a granular material. J. Geophys. Res. 68, 6317-6321 (1963)

Kuster, G., and M. N. Toksoz: Velocity and attenuation of seismic waves in two-phase media: part I. theoretical formulations. Geophysics 39, 587-606 (1974)

Lee, W. B., and S. C. Solomon: Simultaneous inversion of surface wave phase velocity and attenuation: Rayleigh and Love waves over continental and oceanic paths. Bull. Seism. Soc. Am. 69, 65-95 (1979)

Ling, F. F., E. E. Klaus, and R. S. Fein, eds.: Boundary Lubrication: An Appraisal of World Literature. American Society of Mechanical Engineers, N.Y. (1969)

Lockner, D. A., J. B. Walsh, and J. D. Byerlee: Changes in seismic velocity and attenuation during deformation of granite. J. Geophys. Res. 82, 5374-5378 (1977)

McDonal, F. J., F. A. Angona, R. L. Mills, R. L. Sengbush, R. G. van Nostrand, and J. E. White: Attenuation of shear and compressional waves in Pierre shale. Geophysics 23, 421-439 (1958)

Madden, T. R.: Random networks and mixing laws. Geophysics 41, 1104-1125 (1976)

Mavko, G. M.: Frictional attenuation: an inherent amplitude dependence. J. Geophys. Res. in press

Mavko, G. M., and A. Nur: Melt squirt in the asthenosphere. J. Geophys. Res. 80, 1444-1448 (1975)

Mavko, G. M., and A. Nur: Wave attenuation in partially saturated rocks. Geophysics 44, 161-178 (1979)

Merkulova, V. M., E. D. Pigulevskiy, and V. M. Tsaplev: Sound absorption measurements in uniaxially compressed rocks. Physics of the Solid Earth, 166-167 (1972)

Mindlin, R. D., and H. Deresiewicz: Elastic sheres in contact under varying oblique forces. J. Appl. Mech. 20, 327-344 (1953)

Mindlin, R. D., W. P. Mason, T. F. Osmer, and H. Deresiewicz: Effects of an oscillating tangential force on the contact surfaces of elastic spheres. in: Proc. 1st Nat. Congr. Appl. Mech., 203-208 (1952)

Mitchell, B. J.: Regional Rayleigh wave attenuation in North America. J. Geophys. Res. 80, 4904-4916 (1975)

Nowick, A. S., and B. S. Berry: Anelastic Relaxation in Crystalline Solids. Academic Press (1972)

Nur, A., and G. Simmons: The effect of viscosity of a fluid phase on velocity in low porosity rocks. Earth & Planetary Science Letters 7, 99-108 (1969)

O'Connell, R. J., and B. Budiansky: Seismic velocities in dry and saturated cracked solids. J. Geophys. Res. 79, 5412-5426 (1974)

O'Connell, R. J., and B. Budiansky: Viscoelastic properties of fluid-saturated cracked solids. J. Geophys. Res. 82, 5719-5735 (1977)

O'Connell, R. J., and B. Budiansky: Meaures of dissipation in viscoelastic media. Geophys. Res. Letters 5, 5-8 (1978)

Raglan, P. C., J. J. W. Rogers, and P. S. Justus: Origin and differentiation of Triassic dolerite magmas, North Carolina, U.S.A. Contr. Mineral. Petrol. 20, 57-80 (1968)

Rao, M. V. M. S., and Y. V. Ramana: Dilatent behaviour of ultramafic rocks during fracture. Int. J. Rock Mech. Min. Sci. & Geomech. Abstr. 11, 193-203 (1974)

Richter, D., and G. Simmons: Microcracks in crustal igneous rocks: microscopy. in: The Earth's Crust, Its Nature and Physical Properties. Geophysical Monograph 20, Am. Geophys. Union, 149-180 (1977)

Savage, J. C.: Comments on paper by R. B. Gordon and L. A. Davis, "Velocity and attenuation of seismic waves in imperfectly elastic rock". J. Geophys. Res. 74, 726-728 (1969)

Siegfried, R. W., and G. Simmons: Characterization of oriented cracks with differential strain analysis. J. Geophys. Res. 83, 1269-1278 (1978)

Simmons, G., and W. F. Brace: Comparison of static and dynamic measurements of compressibility of rocks. J. Geophys. Res. 70, 5649-5656 (1965)

Simmons, G., and H. W. Cooper: DSA of the Microcracks in GT2 Core: Interpretation and Implications. Technical report to Los Alamos Scientific Laboratory. (1976)

Simmons, G., and H. W. Cooper: Thermal cycling cracks in three igneous rocks. Int. J. Rock Mech. Min. Sci. & Geomech. Abstr. 15, 145-148 (1978)

Simmons, G., and A. Nur: Granites: relation of properties in situ to laboratory measurements. Science 162, 789-791 (1968)

Simmons, G., R. W. Siegfried, and M. Feves: Differential strain analysis: a new method for examining cracks in rocks. J. Geophys. Res. 79, 4383-4385 (1974)

Simmons, G., T. Todd, and W. S. Baldridge: Toward a quantitative relationship between elastic properties and cracks in low porosity rocks. Am. J. of Science 275, 318- 345 (1975)

Sokolnikoff, I. S.: Mathematical Theory of Elasticity (2nd ed.). McGraw-Hill (1956)

Sprunt, E. S., and W. F. Brace: Direct observation of microcavities in crystalline rocks. Int. J. Rock Mech. Min. Sci. 11, 139-150 (1974)

Tabor, D.: Interaction between surfaces: adhesion and friction. in: Surface Physics of Materials, vol II, ed. J. M. Blakely. Academic Press, 475-529 (1975)

Tamai, Y., and B. G. Rightmire: Mechanism of boundary lubrication and the edge effect. J. Basic Engineering 87, 735-739 (1965)

Tittmann, B. R., L. Ahlberg, H. Nadler, J. Curnow, T. Smith, and E. R. Cohen: Internal friction quality factor Q under confining pressure. Proc. 8th Lunar Sci. Conf., Geochim. Cosmochim. Acta Suppl. 8, 1209-1224 (1977)

Tittmann, B. R., J. Curnow, and R. M. Housley: Internal friction quality factor Q > 3100 achieved in lunar rock 70215,85. Proc. Lunar Sci. Conf. 6th, vol. 3, Geochim. Cosmochim. Acta Suppl. 6, 3217-3226 (1975)

Tittmann, B. R., R. M. Housley, G. A. Alers, and E. H. Cirlin: Internal friction in rocks and its relationship to volatiles on the moon. Proc. 5th Lunar Sci. Conf., Geochim. Cosmochim. Acta Suppl. 5, 2913-2918 (1974)

Tittmann, B. R., H. Nadler, J. M. Richardson, and L. Ahlberg: Laboratory measurements of P-wave seismic Q on lunar and analog rocks. Proc. 9th Lunar Planet. Sci. Conf., Geochim. Cosmochim. Acta Suppl. 10, 3627-3635 (1978)

Toksoz, M. N., D. H. Johnston, and A. Timur: Attenuation of seismic waves in dry and saturated rocks: I Laboratory measurements. Geophysics 44, 681-690 (1979)

Volarovich, M. P., and A. S. Gurvich: Investigation of dynamic moduli of elasticity for rocks in relation to temperature. Bull. Acad. Sci. USSR, Geophys. Ser., English Transl. 4, 1-9 (1957)

Walsh, J. B.: The effect of cracks on the compressibility of rock. J. Geophys. Res. 70, 381-389 (1965)

Walsh, J. B.: Seismic wave attenuation in rock due to friction. J. Geophys. Res. 71, 2591-2599 (1966)

Walsh, J. B.: New analysis of attenuation in partially melted rock. J. Geophys. Res. 74, 4333-4337 (1969)

Walsh, J. B., and M. A. Grosenbaugh: A new model for analyzing the effect of fractures on compressibility. J. Geophys. Res. 84, 3532-3536 (1979)

Wang, H. F., and G. Simmons: Microcracks in crystalline rock from 5.3 km depth in the Michigan Basin. J. Geophys. Res. 83, 5849-5856 (1978)

Whitehead, J. R.: Surface deformation and friction of metals at light loads. Proc. Roy. Soc. A201, 109-124 (1950)

Winkler, K., and A. Nur: Pore fluids and seismic attenuation in rocks. Geophys. Res. Letters 6, 1-4 (1979)

Winkler, K., A. Nur, and M. Gladwin: Friction and seismic attenuation in rocks. Nature 277, 528-531 (1979)

Zemanek, J. Jr., and I. Rudnick: Attenuation and dispersion of elastic waves in a cylindrical bar. J. Acoust. Soc. Am. 33, 1283-1288 (1961)

Appendix A

TORSION OF A CYLINDER

The following analysis of the torsion of a cylinder is taken mostly from Hearmon (1961, p 48-51). Consider a cylinder with its axis along the x_3 direction, with one end fixed in the x_1x_2 plane, deformed by a twisting couple applied at the ends (see Fig. A.1). The cylinder will be twisted and the generators of the cylinder will be deformed into helical curves. If the deformation is small, it is assumed that the helical curves can be approximated by straight lines, that is, that the amount of rotation θ is proportional to the distance from the fixed base:

$$\theta = \psi x_3 \tag{A.1}$$

where ψ is the twist per unit length. Displacements, u, in the x_1 and x_2 directions can be found from Fig. A.2:

$$\left.\begin{aligned} u_1 &= r\cos(\theta+\delta) - r\cos\delta = x_1(\cos\theta - 1) - x_2\sin\theta \\ u_2 &= r\sin(\theta+\delta) - r\sin\delta = x_1\sin\theta + x_2(\cos\theta - 1) \end{aligned}\right\} \tag{A.2}$$

where δ is the angle between the radius vector to point $P(x_1,x_2)$ and the x_1 axis. For small angle θ,

$$\left.\begin{aligned} u_1 &= -\theta x_2 \\ u_2 &= \theta x_1 \end{aligned}\right\} \tag{A.3}$$

Since $\theta = \psi x_3$,

$$\left.\begin{aligned} u_1 &= -\psi x_2 x_3 \\ u_2 &= \psi x_1 x_3 \end{aligned}\right\} \tag{A.4}$$

Fig. A.1. Torsion of a cylinder.

Fig. A.2. Cross section of a cylinder in torsion, illustrating the parameters used in the text. After Sokolnikoff (1956, p 107).

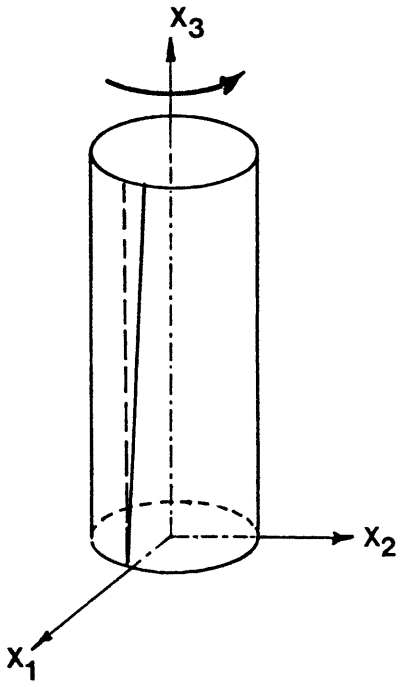
X3
X2
X1

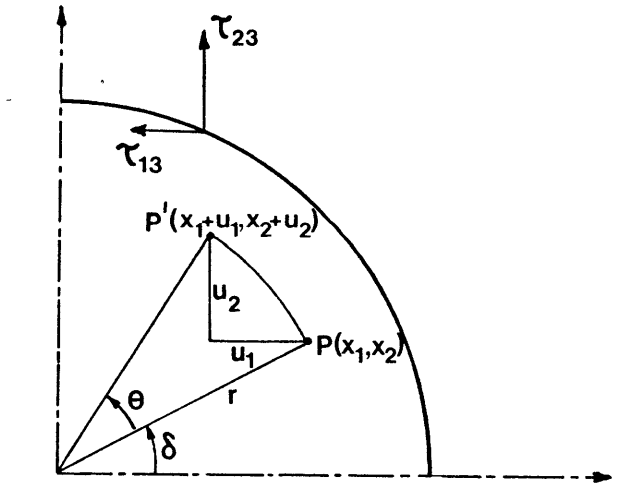
τ23
τ13
P'(x1+u1,x2+u2)
u2
u1
P(x1,x2)
θ
r
δ

The displacement in the x_3 direction is assumed to be

$$u_3 = \psi\phi(x_1,x_2) \tag{A.5}$$

where ϕ is a function describing the warping of the cross section of the twisted cylinder, still to be determined. The strains are given by

$$\varepsilon_{ij} = \frac{1}{2}\left(\frac{\partial u_i}{\partial x_j} + \frac{\partial u_j}{\partial x_i}\right) \tag{A.6}$$

Substituting (A.4) and (A.5) into (A.6), the only non-zero strains are, using the contracted subscript notation,

$$\left.\begin{aligned} S_4 &= 2\varepsilon_{23} = \psi\left(\frac{\partial\phi}{\partial x_2} + x_1\right) \\ S_5 &= 2\varepsilon_{13} = \psi\left(\frac{\partial\phi}{\partial x_1} - x_2\right) \end{aligned}\right\} \tag{A.7}$$

The stresses therefore are given by

$$T_i = c_{i4}S_4 + c_{i5}S_5,\ i = 1,2,\ldots 6 \tag{A.8}$$

If the cylinder is composed of a material with orthorhombic symmetry, with the symmetry axes in the x_1, x_2, and x_3 directions, all c_{i4} and c_{i5} are zero except c_{44} and c_{55} (Hearmon 1961, p. 20). Then

$$\left.\begin{aligned} T_1 &= T_2 = T_3 = T_6 = 0 \\ T_4 &= \psi c_{44}\left(\frac{\partial\phi}{\partial x_2} + x_1\right) \\ T_5 &= \psi c_{55}\left(\frac{\partial\phi}{\partial x_1} - x_2\right) \end{aligned}\right\} \tag{A.9}$$

The function ϕ must be chosen to satisfy the equilibrium equations $\partial T_{ij}/\partial x_j = 0$:

$$\frac{\partial T_5}{\partial x_3} = \frac{\partial T_4}{\partial x_3} = 0 \tag{A.10}$$

showing that T_4 and T_5 are independent of x_3, and

$$\frac{\partial T_5}{\partial x_1} + \frac{\partial T_4}{\partial x_2} = 0 \tag{A.11}$$

which on substituting (A.9) becomes

$$c_{55} \frac{\partial^2 \phi}{\partial x_1^2} + c_{44} \frac{\partial^2 \phi}{\partial x_2^2} = 0 \tag{A.12}$$

(A.12) is solved for ϕ subject to the boundary condition that the surface of the cylinder is stress free,

$$-T_4 \, dx_1 + T_5 \, dx_2 = 0 \tag{A.13}$$

For a circular cylinder, the solution of (A.12) and (A.13) is

$$\phi = x_1 x_2 \frac{c_{55} - c_{44}}{c_{55} + c_{44}} \tag{A.14}$$

From (A.9) and (A.14) the stresses are

$$\left.\begin{aligned} T_4 &= \frac{2\psi c_{44} c_{55} x_1}{(c_{44} + c_{55})} \\ T_5 &= \frac{-2\psi c_{44} c_{55} x_2}{(c_{44} + c_{55})} \end{aligned}\right\} \tag{A.15}$$

From (A.7) and (A.14) the strains are

$$\left.\begin{aligned} S_4 &= \frac{2\psi c_{55} x_1}{(c_{44} + c_{55})} \\ S_5 &= \frac{-2\psi c_{55} x_1}{(c_{44} + c_{55})} \end{aligned}\right\} \tag{A.16}$$

The twisting couple N is given by

$$N = \iint (x_1 T_4 - x_2 T_5) dx_1 dx_2 = \frac{\pi \psi c_{44} c_{55} a^4}{(c_{44} + c_{55})} \tag{A.17}$$

where a is the radius of the cylinder. Since for an orthorhombic material $s_{44} = 1/c_{44}$ and $s_{55} = 1/c_{55}$,

$$N = \frac{\pi\psi a^4}{(s_{44} + s_{55})} \tag{A.18}$$

If the cylinder is isotropic, $c_{44} = c_{55} = G$, the shear modulus, and the stresses, strains and twisting couple become:

$$T_4 = \psi G x_1, \quad T_5 = -\psi G x_2 \tag{A.19}$$

$$S_4 = \psi x_1, \quad S_5 = -\psi x_2 \tag{A.20}$$

$$N = \frac{\pi\psi G a^4}{2} \tag{A.21}$$

Comparing (A.18) and (A.21), we see that the apparent shear modulus of an orthorhombic cylinder with its axis in the x_3 direction is

$$G = \frac{2}{(s_{44}+s_{55})}. \tag{A.22}$$

Appendix B

DETERMINATION OF AMPLITUDE DEPENDENT Q^{-1} FROM TORSIONAL OSCILLATIONS

The specific dissipation factor Q^{-1} is defined by

$$Q^{-1} = \frac{1}{2\pi} \frac{\Delta W}{W} \tag{B.1}$$

where ΔW is the energy loss per cycle per unit volume and W is the peak strain energy per unit volume. For small Q^{-1}, W for torsional oscillations is

$$W = \frac{1}{2} G\varepsilon^2 \tag{B.2}$$

where G is the shear modulus and ε is the strain amplitude. As was shown in Appendix A, for torsional oscillations $\varepsilon = \psi r$, where ψ is the twist per unit length and r is the radial distance from the core axis. Therefore,

$$W(r) = \frac{1}{2} G\psi^2 r^2 \tag{B.3}$$

Combining (B.1) and (B.3), the energy loss per cycle is

$$\Delta W = \pi Q^{-1}(\varepsilon) G\psi^2 r^2 \tag{B.4}$$

where Q^{-1} is now considered to be a function of strain amplitude, and therefore of radius r. For a core of length L and radius *a*, total strain energy is found by integrating (B.3) in cylindrical coordinates:

$$W = \int_0^L dz \int_0^{2\pi} d\theta \int_0^a r dr \left[\frac{1}{2} G\psi^2 r^2\right] = \frac{\pi}{4} G\psi^2 a^4 L \tag{B.5}$$

The total energy loss per cycle for the core is found by integrating (B.4):

$$\Delta W = \int_0^L dz \int_0^{2\pi} d\theta \int_0^a r dr \left[\pi Q^{-1}(\varepsilon) G \psi^2 r^2\right]$$

$$= 2\pi^2 G \psi^2 L \int_0^a r^3 Q^{-1}(\varepsilon) dr \qquad \text{(B.6)}$$

The fractional energy loss per cycle is given by (B.6) divided by (B.5):

$$\frac{\Delta W}{W} = \frac{8\pi}{a^4} \int_0^a r^3 Q^{-1}(\varepsilon) dr \qquad \text{(B.7)}$$

Changing variables in the integral using $\varepsilon = \psi r$,

$$\frac{\Delta W}{W} = \frac{8\pi}{a^4 \psi^4} \int_0^{\psi a} \varepsilon^3 Q^{-1}(\varepsilon) d\varepsilon \qquad \text{(B.8)}$$

The quantity actually measured in the experiment is the amplitude of the rotation of the flywheel, $A = \psi L$. Substituting A for ψ in (B.8) and rearranging,

$$\frac{a^4 A^4 \Delta W}{8\pi L^4 W} = \int_0^{aA/L} \varepsilon^3 Q^{-1}(\varepsilon) d\varepsilon \qquad \text{(B.9)}$$

Differentiating both sides with respect to A,

$$\frac{a^4 A^3}{2\pi L^4} \cdot \frac{\Delta W}{W} + \frac{a^4 A^4}{8\pi L^4} \cdot \frac{d}{dA}\left(\frac{\Delta W}{W}\right) = \frac{a^4 A^3}{L^4} \cdot Q^{-1}\left(\frac{aA}{L}\right) \qquad \text{(B.10)}$$

or,

$$Q^{-1}\left(\frac{aA}{L}\right) = \frac{1}{2\pi} \frac{\Delta W}{W} + \frac{A}{8\pi} \frac{d}{dA}\left(\frac{\Delta W}{W}\right) \qquad \text{(B.11)}$$

Changing from loss per cycle to loss per unit time,

$$\frac{\Delta W}{W} = \frac{1}{f} \cdot \frac{d\ln W}{dt} \tag{B.12}$$

Since W is proportional to the square of the amplitude A,

$$\frac{d\ln W}{dt} = 2\frac{d\ln A}{dt} \tag{B.13}$$

Therefore,

$$Q^{-1}\,\frac{aA}{L} = \frac{1}{\pi f} \cdot \frac{d\ln A}{dt} + \frac{A}{4\pi f} \cdot \frac{d}{dA}\left(\frac{d\ln A}{dt}\right) \tag{B.14}$$

Applying the chain rule to the last term of (B.14),

$$\frac{A}{4\pi f} \cdot \frac{d}{dA}\left(\frac{d\ln A}{dt}\right) = \frac{A}{4\pi f}\left(\frac{dt}{dA}\right) \cdot \frac{d}{dt}\left(\frac{d\ln A}{dt}\right)$$

$$= \frac{1}{4\pi f}\left(\frac{d\ln A}{dt}\right)^{-1} \cdot \left(\frac{d^2 \ln A}{dt^2}\right) \tag{B.15}$$

Therefore, (B.14) becomes

$$Q^{-1}\,\frac{aA}{L} = \frac{1}{\pi f} \cdot \frac{d\ln A}{dt} + \frac{1}{4\pi f}\left(\frac{d\ln A}{dt}\right)^{-1}\left(\frac{d^2 \ln A}{dt^2}\right) \tag{B.16}$$

If Q^{-1} is amplitude independent, then dlnA/dt is a constant and (B.16) becomes the usual equation,

$$Q^{-1} = \frac{1}{\pi f} \cdot \frac{d\ln A}{dt} \tag{B.17}$$

If Q^{-1} is amplitude dependent, (B.16) can be used to calculate Q^{-1} for the strain amplitude at the surface of the sample, aA/L.

Appendix C

SHEAR MODULI OF SOME OF THE SAMPLES

In the following tables are listed the shear moduli of those samples for which it was possible to make the calculation from the sample dimensions and the frequency of the torsional oscillation, according to Eq. 5.19:

$$G = \frac{8\pi f^2 LJ}{a^4}$$

where G is the shear modulus, f is the frequency, L is the sample length, J is the moment of inertia of the flywheel, and a is the sample radius. Unfortunately, for the rest of the attenuation measurements, I did not record the sample length, so that the shear modulus cannot be calculated, except for the variations of G with direction in Westerly granite, discussed in Sec. 5.5.

The above equation applies to the case where a twisting couple is applied to the ends of the sample. For the measurements made here, the sample was clamped along a portion of its length at each end, so that the above equation anly applies approximately. Because of the end effects due to the clamping, the effective length of the sample is not necessarily the same as the distance between the chucks. Therefore, the actual values of G should be considered to be approximate, although the variations in G are significant.

Table C.1. Shear modulus of sample 1401 as a function of temperature. Only variations in the last digit of G are significant.

Temperature, °C	G, Mbar
27	0.240
95	0.237
140	0.236
27	0.241
95	0.236
180	0.234
270	0.229
355	0.223
440	0.212
520	0.204
26	0.220
95	0.218
185	0.213
270	0.205
355	0.201
435	0.197
525	0.196
25	0.215

Table C.2. Shear modulus of sample 1407, Middlebrook felsite, as a function of temperature. Only variations in the last digit of G are significant.

Temperature, °C	G, Mbar	Temperature, °C	G, Mbar
25	0.234	26	0.195
50	0.234	105	0.194
70	0.234	190	0.191
95	0.233	275	0.187
115	0.232	360	0.185
135	0.231	445	0.181
160	0.229	525	0.169
185	0.227	610	0.129
360	0.224	525	0.131
440	0.212	440	0.146
520	0.181	360	0.148
435	0.193	280	0.147
350	0.202	190	0.146
275	0.205	100	0.147
185	0.204	25	0.144
100	0.200		

Table C.3. Shear modulus and crack density of thermally cycled Westerly granite. All cores have their axes in the hardway direction. Crack density ϵ was calculated from the room dry shear modulus using the equations for dry rocks from Budiansky and O'Connell (1976):

$$\frac{\bar{G}}{G} = 1 - \frac{32(1-\bar{\nu})(5-\bar{\nu})}{45(2-\bar{\nu})}\,\epsilon$$

$$\epsilon = \frac{45\,(\nu-\bar{\nu})(2-\bar{\nu})}{16(1-\bar{\nu}^2)(10\nu-3\nu\bar{\nu}-\bar{\nu})}$$

where G is the intrinsic shear modulus, $\bar{G}$ is the effective shear modulus, ν is the intrinsic Poisson's ratio, and $\bar{\nu}$ is the effective Poisson's ratio. Values of G = 0.34 Mbar and ν = 0.21 from Simmons and Brace (1965) for Westerly granite at 10 kbar were used. Crack density was found by assuming G and ν and solving the above equations iteratively using the measured $\bar{G}$. The value of ϵ for the uncycled core, 0.34, calculated from the shear modulus, agrees well with the value of 0.35 calculated from the compressibility (see Table 3.1). The measured shear moduli of the saturated cores were less than for the dry case while the theory predicts that the saturated shear modulus should be greater that the dry case. This discrepancy has not yet been resolved.

Table C.3 continued

maximum cycling temperature, °C	crack porosity x 10^6 (±25%)	G, Mbar saturated	G, Mbar dry	crack density ϵ
25	1450	0.148	0.118	0.34
130	2480	0.132	0.114	0.36
229	4100	0.102	0.079	0.41
326	6800	0.081	0.073	0.44
433	11,700	0.056	0.051	0.48
486	15,300	0.047	0.043	0.49

GLOSSARY

rift, grain, and hardway directions: used in the discussion of anisotropy of Q^{-1} in Secs. 4.3 and 5.5, the rift, grain, and hardway directions are perpendicular to the rift, grain, and hardway planes respectively, which are quarrying terms for the planes of easiest, intermediate, and hardest splitting of the rock.